

Robust Data-Driven Predictive Control for Mixed Platoons under Noise and Attacks

Shuai Li, Chaoyi Chen, Haotian Zheng, Jiawei Wang, Qing Xu, Jianqiang Wang, and Keqiang Li

Abstract—Controlling mixed platoons, which consist of both connected and automated vehicles (CAVs) and human-driven vehicles (HDVs), poses significant challenges due to the uncertain and unknown human driving behaviors. Data-driven control methods offer promising solutions by leveraging available trajectory data, but their performance can be compromised by noise and attacks. To address this issue, this paper proposes a Robust Data-Enabled Predictive Leading Cruise Control (RD_{ee}P-LCC) framework based on data-driven reachability analysis. The framework over-approximates system dynamics under noise and attack using a matrix zonotope set derived from data, and develops a stabilizing feedback control law. By decoupling the mixed platoon system into nominal and error components, we employ data-driven reachability sets to recursively compute error reachable sets that account for noise and attacks, and obtain tightened safety constraints of the nominal system. This leads to a robust data-driven predictive control framework, solved in a tube-based control manner. Numerical simulations and human-in-the-loop experiments demonstrate that the RD_{ee}P-LCC method significantly improves robustness against noise and attacks, while enhancing tracking accuracy, control efficiency, energy economy, and driving comfort.

Index Terms—Connected and automated vehicles, mixed platoon, data-driven control, robust control, human-in-the-loop.

I. INTRODUCTION

RECENT advancements in connected and automated vehicles (CAVs) have led to the increasing deployment of vehicles featuring various levels of autonomous driving capabilities in public transportation systems [1], [2]. Among these innovations, adaptive cruise control (ACC) has emerged as a significant implementation, reducing the need for constant driver intervention in speed management [3] and enhancing proactive driving safety [4]. Despite these benefits, recent empirical and experimental studies [5], [6] have revealed the inherent limitations of ACC in optimizing traffic flow. These limitations are primarily attributed to ACC's over-conservative car-following policy and short-sighted perception capabilities [7].

This work was supported by the National Natural Science Foundation of China under Grant 52221005, the National Natural Science Foundation of China under Grant 52302410, the China Postdoctoral Science Foundation under Grant 2024T170489, the Postdoctoral Fellowship Program of CPSF under Grant GZB20230354, the Research and Development of Autonomous Driving Domain Controller and Its Algorithm under Grant 2023Z070, and the Shuimu Tsinghua Scholarship. Corresponding author: Keqiang Li and Jiawei Wang.

S. Li, H. Zheng, C. Chen, Q. Xu, J. Wang, and K. Li are with the School of Vehicle and Mobility, Tsinghua University, Beijing, China. ({li-s21, zhenght24}@mails.tsinghua.edu.cn, {chency2023, qingxu, wjqlws, likq}@tsinghua.edu.cn).

J. Wang is with the Department of Civil and Environmental Engineering, University of Michigan, Ann Arbor, USA. (jiawe@umich.edu).

In contrast to ACC, cooperative adaptive cruise control (CACC) employs vehicle-to-vehicle (V2V) communication to organize multiple CAVs as a pure CAV platoon and apply cooperative control methods [8]. This approach shows substantial potential in improving traffic performance, including traffic stability [9], road capacity [10], energy efficiency [11]. However, the effectiveness of CACC is hindered by the requirement for all the involved vehicles to possess autonomous capabilities. In practice, mixed traffic environments, where CAVs and human-driven vehicles (HDVs) coexist, are expected to persist for an extended period [12]. At low CAV penetration rates, the probability of consecutive vehicles being equipped with CAV technology becomes negligible [13], [14]. To overcome the limitations of pure CAV platoons in mixed traffic, mixed platooning has emerged as a promising alternative, which integrates both CAVs and HDVs in a platoon [15]–[17]. The core idea is to guide the behavior of HDVs by directly controlling CAVs, thereby enhancing overall traffic performance [18], [19]. Recent studies, including traffic simulations [20], [21], hardware-in-the-loop tests [22], [23], and real-world experiments [18], [24], have shown the potential benefits of mixed platoons for smoothing traffic flow and improving traffic efficiency, even at low CAV penetration rates.

To achieve these benefits while preserving CAV safety, existing research on mixed platoon control mainly relies on model-based control methods. These methods utilize microscopic car-following models, such as the intelligent driver model (IDM) [25] and optimal velocity model (OVM) [26], to capture the longitudinal behavior of HDVs. Parametric models are then derived to represent the dynamics of the entire mixed platoon system, enabling the implementation of various model-based control strategies, including linear quadratic regulator [15], structured optimal control [19], model predictive control (MPC) [27], adaptive control [28], \mathcal{H}_∞ robust control [29], and control barrier function [30]. However, the inherent randomness and uncertainty in the car-following behavior of HDVs present a significant challenge in accurately identifying the mixed platoon dynamics. The resulting model mismatches may limit the performance of these model-based techniques. On the other hand, model-free or data-driven methods have gained increasing attention [31]–[34]. Approaches like adaptive dynamic programming [31], [32] and reinforcement learning [20], [33] have shown potential in learning CAV control policies through iterative training, without the necessity of a previous knowledge about the dynamics of mixed platoons. However, it is worth noting that safety is always prioritized first for CAVs, but these

methods lack principled safety constraints, as they typically take an indirect manner by penalizing unsafe actions in the reward function. Although recent advancements, such as safe reinforcement learning, have begun to formally address safety concerns in mixed platoons [35], [36], these methods still face significant challenges, including high computational demands and limited generalization capabilities.

For deriving safe and optimal control inputs directly from data, one promising approach is data-driven predictive control, with the combination of the well-established MPC and data-driven techniques [37]. Along this direction, several methods have been proposed for data-driven mixed platoon control [38]–[41], with a notable example being Data-Enabled Predictive Control (DeePC) [42]. Specifically, DeePC represents the system behavior in a data-centric manner via Willems’ fundamental lemma [43], and incorporates explicit input-output constraints in online predictive control optimization. By adapting DeePC to a Leading Cruise Control (LCC) framework [44], which is particularly designed for mixed traffic, the recently proposed Data-Enabled Predictive Leading Cruise Control (DeeP-LCC) allows for CAVs’ safe and optimal control in mixed platoons [39]. The effectiveness of this approach has been validated across multiple dimensions, including the mitigation of traffic waves [39], the reduction of energy consumption [45], and the enhancement of privacy protection [46]. However, real-world data are always corrupted by noise from vehicle perception systems or V2X communication channels. Moreover, these data-driven CAV control systems become increasingly vulnerable to attacks in the V2X network, which may maliciously alter control inputs or perceived data to execute attacks [47], thereby compromising CAV control safety. Existing research tends to overlook the influence of noise on data collection and online predictive control, and often assumes the absence of adversarial attacks. This assumption could limit the CAV’s ability to effectively follow desired trajectories and may raise significant safety concerns [48].

To explicitly address noise and attacks, growing evidence has indicated that robustness is crucial in standard DeePC [49], [50]. Indeed, a recent paper has reformulated DeeP-LCC using min-max robust optimization to handle unknown disturbances [51]. However, prior assumptions on disturbances are still needed to improve computational efficiency. Compared to the min-max approach, reachability analysis offers a more computationally reliable method for ensuring robustness against a wide range of noise and attacks. Several recent works have applied similar techniques to design robust control strategies for CAVs, including anti-attack control employing reach-avoid specification [47] and formal safety net control using backward reachability analysis [52]. Note that most of these methods are model-based, with one notable exception of [38], which presents a zonotopic predictive control (ZPC) approach. Nonetheless, the prediction accuracy in [38] may be limited by the utilization of over-approximated data-driven dynamics. Moreover, the boundaries of noise and attack have not been well-explored in [38], which could significantly affect the performance of data-driven predictive control.

To address the aforementioned research gaps, this paper pro-

poses a Robust Data-Enabled Predictive Leading Cruise Control (RDDeP-LCC) method that leverages data-driven reachability analysis. The goal is to develop robust control strategies for CAVs against noise and attacks in mixed platoons. We introduce specific evaluation indices to comprehensively analyze RDDeP-LCC’s tracking performance under different boundary conditions. Additionally, human-in-the-loop experiments are conducted to provide near-real-world validation. Some preliminary results have been outlined in [53]. Precisely, the main contributions of this paper are as follows:

- 1) We propose a novel RDDeP-LCC formulation for mixed platoon control that explicitly addresses noise and attacks. Inspired by [38], [54], we capture noise and attacks as zonotope sets, in contrast to the zero assumption in [39]. We decouple the system into nominal and error subsystems and use matrix zonotope set techniques to build an over-approximated error reachable set. By subtracting this set from the system constraints, we derive a tightened nominal reachable set, which is used as a safety constraint to reformulate the standard DeeP-LCC problem. The nominal control input is computed accordingly, and the actual control input for the CAV is obtained via a tube-based control manner, combining nominal and error feedback control inputs to enhance safety and robustness.
- 2) We then perform numerical simulations to compare the control performance of RDDeP-LCC with baseline methods, including standard MPC, standard DeeP-LCC, and ZPC. Specifically, our analysis focuses on quantifying the impact of varying noise and attack boundaries on platoon tracking performance. The simulation results show that, without explicitly addressing noise and adversarial attacks, standard DeeP-LCC performs even worse than traditional all-HDV traffic. In contrast, the proposed RDDeP-LCC consistently outperforms the baseline methods under various noise and attack boundary conditions, demonstrating its significant robustness improvements for data-driven control techniques in mixed traffic systems.
- 3) Finally, human-in-the-loop experiments are conducted with real human drivers engaged using driving simulators, whereas existing research primarily relies on simulations with HDVs represented by recorded data or car-following models. Results show that standard DeeP-LCC fails to stabilize mixed traffic under noise and attack conditions. By contrast, RDDeP-LCC outperforms the baseline methods, reducing velocity deviations by 26.1%, real cost by 24.7%, fuel consumption by 11.4%, and improving driving comfort by 26.0%, compared to all-HDV traffic, respectively. These results highlight the superior robustness and practical effectiveness of RDDeP-LCC in controlling mixed platoons against common noise and adversarial attacks.

The remainder of this paper is organized as follows: Section II introduces the problem statement and preliminaries. Section III presents the RDDeP-LCC formulation. Section IV shows numerical simulations. Human-in-the-loop experiments are provided in Section V, and Section VI concludes this paper.

II. PROBLEM STATEMENT

In this section, we first introduce the research scenario, and then give the parametric model of the mixed platoon system under the LCC framework [44].

A. Research Scenario

Based on the spatial distribution of CAVs, large-scale mixed traffic systems can be naturally partitioned into multiple mixed platoons with the Leading Cruise Control (LCC) topology [44] using a decentralized traffic control framework [55]. In this context, achieving robust control for each mixed platoon is essential to ensure the overall stability and efficiency of the traffic system. As illustrated in Fig. 1, each mixed platoon system comprising one leading CAV (indexed as 1) and $n - 1$ following HDVs (indexed as $2, \dots, n$ against the moving direction), and all vehicles in the platoon follow a head vehicle (HV) (indexed as 0).

In this study, we consider a control framework for mixed platoons, which could be deployed in an edge cloud control platform. Precisely, we assume that roadside units can acquire state data for all the vehicles and transmit it to the cloud control platform without delay. Then, a specific controller within the cloud calculates the control commands, which are sent to the CAVs to regulate mixed platoons. It is worth noting that for platoon control, a small variation in the velocity of the head vehicle could necessitate a corresponding and synchronized adjustment in the velocity for all subsequent vehicles to maintain operational safety. Given the fact that only the CAV is under direct control in mixed platoons, the dynamic process of velocity adaptation poses substantial challenges, particularly in scenarios where the system is subject to noise and attacks. Under such conditions, the effective control of CAVs becomes crucial to ensure the safety and stability of the entire mixed platoon. Accordingly, the main research focus of this paper is to develop a robust data-driven control framework for CAVs that can effectively mitigate the impact of noise and attacks. Particularly, as shown in Fig. 1, we assume that the noise affects the observation process of the system state in the cloud control platform, while the attacks inject the control input received by the CAVs.

Remark 1: For large-scale mixed traffic, our method can be extended through a decentralized manner based on spatial segmentation [55]. Specifically, the traffic flow is partitioned into multiple mixed platoons, where each platoon is consisted of one CAV and $n - 1$ following HDVs. This partition is naturally determined by the spatial locations of the CAVs in mixed traffic. Then, the proposed method decomposition transforms the original high-dimensional, multi-input system into multiple lower-dimensional, single-input subsystems, significantly reducing both system complexity and computational burden. Consequently, this facilitates the efficient design and real-time implementation of the control algorithm. Moreover, the distributed nature of this strategy ensures inherent scalability, enabling it to adapt effectively to traffic systems with varying sizes.

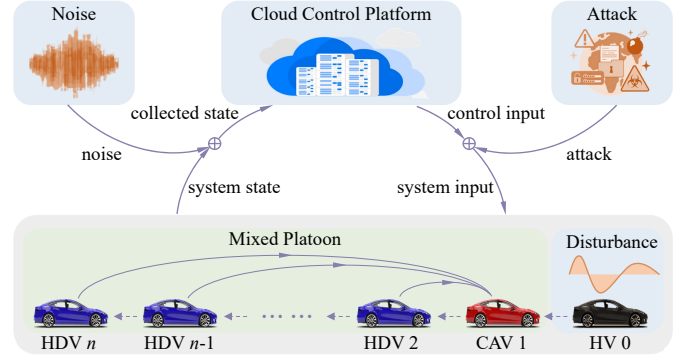


Fig. 1. Schematic for mixed platoon under the influence of noise and attacks. The blue, red, and black vehicles are HDVs, CAV, and head vehicle, respectively. The blue and green boxes represent the head vehicle and mixed platoon, respectively. The noise and attacks affect the uplink and downlink of the cloud control platform, respectively.

B. Parametric Model of Mixed Platoon System

In the following, we introduce the parametric modeling process for mixed platoons, which is commonly used in model-based methods. For each vehicle $i \in \Omega$, the spacing error $\tilde{s}_i(t)$ and velocity error $\tilde{v}_i(t)$ are defined as state variables:

$$\begin{cases} \tilde{s}_i(t) = s_i(t) - s_i^*, \\ \tilde{v}_i(t) = v_i(t) - v_i^*, \end{cases} \quad (1)$$

where $s_i(t)$ and $v_i(t)$ denote the spacing and velocity of vehicle i , while s_i^* and v_i^* represent their corresponding equilibrium values.

For HDVs, we adopt a linearized car-following model based on well-established formulations, such as IDM [25] and OVM [26]. The resulting dynamics for HDVs are given by:

$$\begin{cases} \dot{\tilde{s}}_i(t) = \tilde{v}_{i-1}(t) - \tilde{v}_i(t), \\ \dot{\tilde{v}}_i(t) = \gamma_{i,1}\tilde{s}_i(t) + \gamma_{i,2}\tilde{v}_i(t) + \gamma_{i,3}\tilde{v}_{i-1}(t), \end{cases} \quad (2)$$

where $\gamma_{i,1}$, $\gamma_{i,2}$, and $\gamma_{i,3}$ are linearized model coefficients.

For CAVs, we consider the scenario where the control input is subject to false data injection attacks. Under such conditions, the linearized dynamics can be expressed as:

$$\begin{cases} \dot{\tilde{s}}_i(t) = \tilde{v}_{i-1}(t) - \tilde{v}_i(t), \\ \dot{\tilde{v}}_i(t) = u_i(t) + \vartheta_i(t), \end{cases} \quad (3)$$

where $u_i(t)$ is the designed control input for CAVs, and $\vartheta_i(t)$ represents the attack acting on the control input. The modeling of such attack scenarios follows prior research in [47], [56].

We define $x_i(t) = [\tilde{s}_i(t), \tilde{v}_i(t)]^\top$ as the state for vehicle i , and lump the states of all vehicles to obtain the system state $x(t) = [x_1^\top(t), x_2^\top(t), \dots, x_n^\top(t)]^\top \in \mathbb{R}^{2n \times 1}$. By combining (2) and (3), the state-space model of the mixed platoon is obtained as:

$$\dot{x}(t) = A_{\text{con}}x(t) + B_{\text{con}}u(t) + H_{\text{con}}\epsilon(t) + J_{\text{con}}\vartheta(t), \quad (4)$$

where $u(t) = u_1(t) \in \mathbb{R}$ and $\vartheta(t) = \vartheta_1(t) \in \mathbb{R}$ represents the control input and attack for the CAV, $\epsilon(t) = \tilde{v}_0(t) = v_0(t) - v_0^*(t) \in \mathbb{R}$ is the disturbance from the head vehicle. The matrices $A_{\text{con}} \in \mathbb{R}^{2n \times 2n}$, $B_{\text{con}} \in \mathbb{R}^{2n \times 1}$, $H_{\text{con}} \in \mathbb{R}^{2n \times 1}$, and $J_{\text{con}} \in \mathbb{R}^{2n \times 1}$ represent the system matrix, the control matrix,

the disturbance matrix, and the attack matrix, are defined as follows respectively:

$$\begin{bmatrix} A_1 & & & \\ D_2 & A_2 & & \\ & \ddots & \ddots & \\ & & D_i & A_i \\ & & & \ddots & \ddots \\ & & & & D_n & A_n \end{bmatrix}, \begin{bmatrix} B_1 \\ B_2 \\ \vdots \\ B_i \\ \vdots \\ B_n \end{bmatrix}, \begin{bmatrix} H_1 \\ H_2 \\ \vdots \\ H_i \\ \vdots \\ H_n \end{bmatrix}, \begin{bmatrix} J_1 \\ J_2 \\ \vdots \\ J_i \\ \vdots \\ J_n \end{bmatrix}, \quad (5)$$

with sub-block matrices within (5) is given as follows:

$$A_1 = \begin{bmatrix} 0 & -1 \\ 0 & 0 \end{bmatrix}, A_i = \begin{bmatrix} 0 & -1 \\ \gamma_{i,1} & -\gamma_{i,2} \end{bmatrix}, D_i = \begin{bmatrix} 0 & 1 \\ 0 & \gamma_{i,3} \end{bmatrix}, \\ B_1 = \begin{bmatrix} 0 \\ 1 \end{bmatrix}, H_1 = \begin{bmatrix} 1 \\ 0 \end{bmatrix}, J_1 = \begin{bmatrix} 0 \\ 1 \end{bmatrix}, B_i = H_i = J_i = \begin{bmatrix} 0 \\ 0 \end{bmatrix}. \quad (6)$$

Subsequently, the continuous system in (4) can be discretized employing the forward Euler method, taking into account noise $\omega(k)$, resulting in the discrete model:

$$x(k+1) = Ax(k) + Bu(k) + H\epsilon(k) + J\vartheta(k) + \omega(k), \quad (7)$$

where k represents the discrete time step, A , B , H , and J are the corresponding discrete-time system matrices.

Motivated by the existing research [47], [57]–[59], we assume that the disturbance $\epsilon(k)$, the attack $\vartheta(k)$, and the noise $\omega(k)$, are norm bounded. These conditions are formally expressed as:

$$\|\epsilon(k)\|_\infty \leq \epsilon_{\max}, \quad \|\vartheta(k)\|_\infty \leq \vartheta_{\max}, \quad \|\omega(k)\|_\infty \leq \omega_{\max}, \quad (8)$$

where ϵ_{\max} , ϑ_{\max} , and ω_{\max} denote the respective upper bounds. Note that these bounds must be known a priori, as they are essential for the offline construction of the over-approximated system matrix set (15) and the online computation of the data-driven reachable set (28), as detailed in Section III.

Remark 2: Although the typical car-following models can capture the driving behavior of human drivers, human's uncertain nature makes it non-trivial to accurately identify the model (7) involving HDVs. Accordingly, the system matrices A , B , H , and J are uncertain and unknown, which motivates us to develop a data-driven predictive control method to obtain the optimal control input $u(k)$ for CAVs. Note that the model (7), which is indeed unknown, is only used to clarify the dimensions and physical meaning of state and control variables in this paper, facilitating our design of the data-driven dynamics and reachability analysis in Section III.

Remark 3: In this paper, we do not explicitly identify the model of false data injection attacks, as such attacks are often unpredictable and difficult to characterize [59], [60]. Instead, we consider a general class of attacks where the injected signal $\vartheta(k)$ is bounded and may be either state-dependent or state-independent, without assuming any specific structure or distribution. This general formulation enhances the applicability of the proposed method to a broader range of adversarial scenarios.

C. Preliminaries and Theoretical Foundations

Before proceeding, we introduce the necessary preliminaries on data-driven predictive control and reachable sets, which form the foundation of our proposed approach. The data-driven predictive control method employed in this paper is based on Willems' fundamental lemma and Hankel matrices, with relevant definitions provided in [43, Theorem 1] and [42, Definition 4.4]. For the computation of reachable sets, we utilize zonotope sets to describe the reachable sets for efficient computation [54]. Some basic definitions are presented below.

Definition 1 (Interval Set [61]): An interval set \mathcal{I} is a connected subset of \mathbb{R}^n , and it can be defined as $\mathcal{I} = \{x_{\mathcal{I}} \in \mathbb{R}^n \mid \underline{x}_{\mathcal{I}} \leq x_{\mathcal{I}} \leq \bar{x}_{\mathcal{I}} \quad \forall i = 1, \dots, n\}$, where $\underline{x}_{\mathcal{I}}$ and $\bar{x}_{\mathcal{I}}$ are the lower bound and upper bound of $x_{\mathcal{I}}$, respectively. Interval set can be represented as $\mathcal{I} = [\underline{\mathcal{I}}, \bar{\mathcal{I}}]$, with $\underline{\mathcal{I}} = [\underline{x}_{\mathcal{I}_1}, \underline{x}_{\mathcal{I}_2}, \dots, \underline{x}_{\mathcal{I}_n}]$ and $\bar{\mathcal{I}} = [\bar{x}_{\mathcal{I}_1}, \bar{x}_{\mathcal{I}_2}, \dots, \bar{x}_{\mathcal{I}_n}]$.

Definition 2 (Zonotope Set [62]): Given a center vector $c_{\mathcal{Z}} \in \mathbb{R}^n$, and $\gamma_{\mathcal{Z}} \in \mathbb{N}$ generator vectors in a generator matrix $G_{\mathcal{Z}} = [g_{\mathcal{Z}}^{(1)}, g_{\mathcal{Z}}^{(2)}, \dots, g_{\mathcal{Z}}^{(\gamma_{\mathcal{Z}})}] \in \mathbb{R}^{n \times \gamma_{\mathcal{Z}}}$, a zonotope set is defined as $\mathcal{Z} = \langle c_{\mathcal{Z}}, G_{\mathcal{Z}} \rangle = \{x \in \mathbb{R}^n \mid x = c_{\mathcal{Z}} + \sum_{i=1}^{\gamma_{\mathcal{Z}}} \beta^{(i)} g_{\mathcal{Z}}^{(i)}, -1 \leq \beta^{(i)} \leq 1\}$. For zonotope sets, the following operations hold:

- *Linear Map:* For a zonotope set $\mathcal{Z} = \langle c_{\mathcal{Z}}, G_{\mathcal{Z}} \rangle$, $L \in \mathbb{R}^{m \times n}$, the linear map is defined as $L\mathcal{Z} = \langle Lc_{\mathcal{Z}}, LG_{\mathcal{Z}} \rangle$.
- *Minkowski Sum:* Given two zonotope sets $\mathcal{Z}_1 = \langle c_{\mathcal{Z}_1}, G_{\mathcal{Z}_1} \rangle$ and $\mathcal{Z}_2 = \langle c_{\mathcal{Z}_2}, G_{\mathcal{Z}_2} \rangle$ with compatible dimensions, the Minkowski sum is defined as $\mathcal{Z}_1 + \mathcal{Z}_2 = \langle c_{\mathcal{Z}_1} + c_{\mathcal{Z}_2}, [G_{\mathcal{Z}_1}, G_{\mathcal{Z}_2}] \rangle$.
- *Cartesian Product:* Given two zonotope sets $\mathcal{Z}_1 = \langle c_{\mathcal{Z}_1}, G_{\mathcal{Z}_1} \rangle$ and $\mathcal{Z}_2 = \langle c_{\mathcal{Z}_2}, G_{\mathcal{Z}_2} \rangle$, the cartesian product is defined as

$$\mathcal{Z}_1 \times \mathcal{Z}_2 = \left\langle \begin{bmatrix} c_{\mathcal{Z}_1} \\ c_{\mathcal{Z}_2} \end{bmatrix}, \begin{bmatrix} G_{\mathcal{Z}_1} & 0 \\ 0 & G_{\mathcal{Z}_2} \end{bmatrix} \right\rangle.$$

- *Over-Approximated Using Interval Set:* A zonotope set $\mathcal{Z} = \langle c_{\mathcal{Z}}, G_{\mathcal{Z}} \rangle$ could be over-approximated by an interval set $\mathcal{I} = [c_{\mathcal{Z}} - \Delta g_{\mathcal{Z}}, c_{\mathcal{Z}} + \Delta g_{\mathcal{Z}}]$, where $\Delta g_{\mathcal{Z}} = \sum_{i=1}^{\gamma_{\mathcal{Z}}} |g_{\mathcal{Z}}^{(i)}|$.

Definition 3 (Matrix Zonotope Set [61]): Given a center matrix $C_{\mathcal{M}} \in \mathbb{R}^{n \times m}$, and $\gamma_{\mathcal{M}} \in \mathbb{N}$ generator matrices in a generator matrix $G_{\mathcal{M}} = [G_{\mathcal{M}}^{(1)}, G_{\mathcal{M}}^{(2)}, \dots, G_{\mathcal{M}}^{(\gamma_{\mathcal{M}})}] \in \mathbb{R}^{n \times m \gamma_{\mathcal{M}}}$, a matrix zonotope set is defined as $\mathcal{M} = \langle C_{\mathcal{M}}, G_{\mathcal{M}} \rangle = \{X \in \mathbb{R}^{n \times m} \mid X = C_{\mathcal{M}} + \sum_{i=1}^{\gamma_{\mathcal{M}}} \beta^{(i)} G_{\mathcal{M}}^{(i)}, -1 \leq \beta^{(i)} \leq 1\}$.

Definition 4 (Reachable Set): For the discrete control system (7), the reachable set \mathcal{R}_{k+1} of system state at time step $k+1$ is defined as:

$$\mathcal{R}_{k+1} = \{x(k+1) \in \mathbb{R}^{2n} \mid x(k+1) = Ax(k) + Bu(k) + H\epsilon(k) + J\vartheta(k) + \omega(k), x(k) \in \mathcal{R}_k, u(k) \in \mathcal{Z}_{u_k}, \epsilon(k) \in \mathcal{Z}_{\epsilon_k}, \vartheta(k) \in \mathcal{Z}_{\vartheta_k}, \omega(k) \in \mathcal{Z}_{\omega_k}\}, \quad (9)$$

where \mathcal{R}_k is the reachable set at time step k , and \mathcal{Z}_{u_k} , \mathcal{Z}_{ϵ_k} , $\mathcal{Z}_{\vartheta_k}$, and \mathcal{Z}_{ω_k} are the admissible zonotope sets for $u(k)$, $\epsilon(k)$, $\vartheta(k)$, and $\omega(k)$ at time step k , respectively.

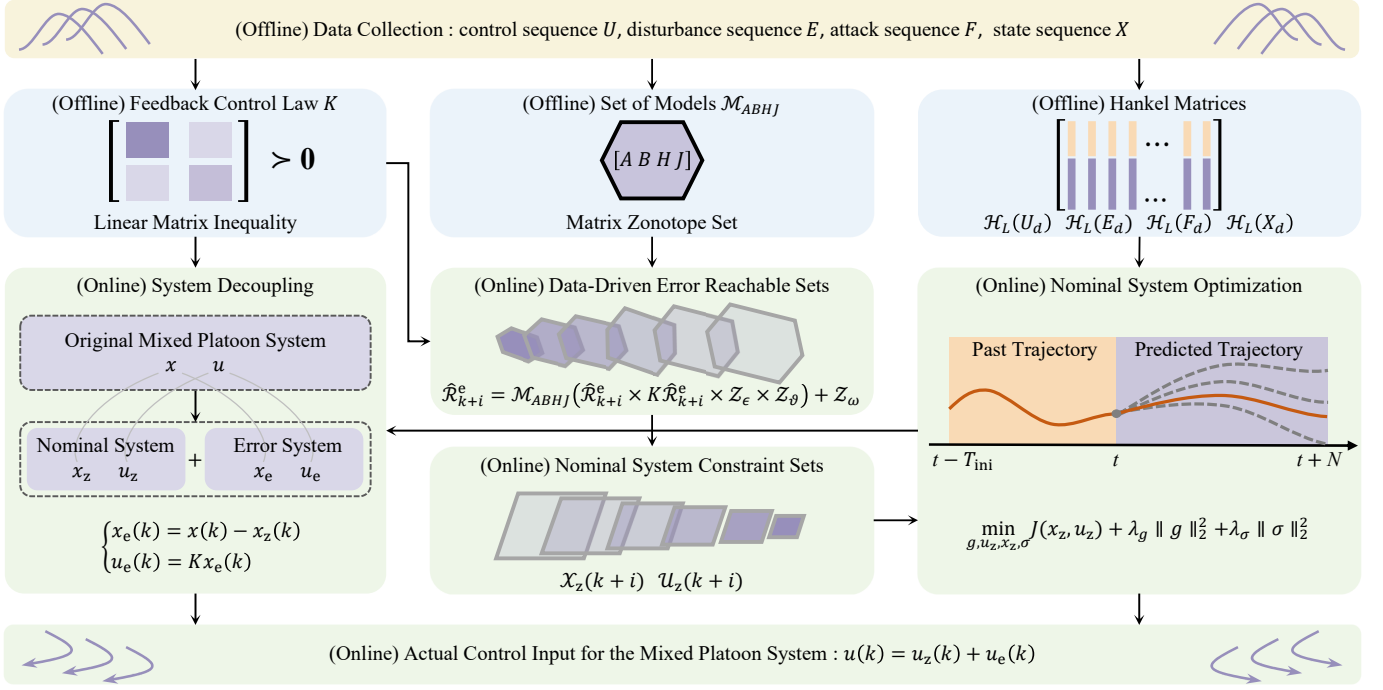


Fig. 2. Schematic of the proposed RDDeP-LCC method for mixed platoons. In the offline learning phase (blue), the method utilizes pre-collected data (yellow) to calculate the over-approximated system matrix set \mathcal{M}_{ABHJ} , derive a data-driven feedback control law K to ensure stability for all possible systems, and generate the Hankel matrices. In the online control phase (green), the RDDeP-LCC solves for optimal control input for the CAV in a receding horizon strategy. Specifically, The system is decomposed into the error system and the nominal system. Using \mathcal{M}_{ABHJ} and K , the method recursively derives the data-driven reachable set of error states, and then subtracts this set from the constraints of the original system to obtain a more compact nominal system constraint. Then, the nominal control input $u_z(k)$ is calculated using the standard DeeP-LCC under the compact nominal constraint. Finally, the actual control input of the CAV is obtained by combining the nominal control input $u_z(k)$ with the error feedback control input $u_e(k)$ in a tube-based control manner.

III. METHODOLOGY

This section proposes the Robust Data-Enabled Predictive Leading Cruise Control (RDDeP-LCC) method for mixed platoon control, as shown in Fig. 2. Precisely, RDDeP-LCC consists of three main phases:

1) **Data Collection:** Pre-collected data includes the control inputs $u(k)$ of the CAVs, the velocity error $\epsilon(k)$ of the head vehicle, the adversarial attacks $\vartheta(k)$, and the states $x(k)$ of all vehicles in the mixed platoon system, all under the influence of the unknown noise $\omega(k)$ (see Section III-A).

2) **Offline Learning:** Pre-collected data is employed to construct an over-approximated system matrix set \mathcal{M}_{ABHJ} , capturing the unknown and uncertain dynamics of the mixed platoon. A data-driven feedback control law K from data is then derived to ensure stability across all systems. Both \mathcal{M}_{ABHJ} and K are later used in the online control phase to compute the data-driven reachable set. The pre-collected data also forms Hankel matrices, which are part of the data-driven model used in online control (see Section III-B).

3) **Online Control:** The actual mixed platoon system is decoupled into an error component and a nominal component, motivated by tube-based control strategies. Based on \mathcal{M}_{ABHJ} and K , we recursively compute the data-driven reachable sets of error states within the prediction horizon. This reachable set is then subtracted from the original system constraints to obtain a more compact nominal system constraint. Based on the obtained compact nominal system constraint, the standard DeeP-LCC in [39] is reformulated for online optimization

in RDDeP-LCC, solving which provides the nominal control input $u_z(k)$. Finally, the actual control input of the CAV is obtained by combining the $u_z(k)$ with the error feedback control input $u_e(k)$ in a tube-based control manner. The resulting RDDeP-LCC controller promises safe and robust control, even in the presence of noise and attacks (see Section III-C).

A. Data Collection

In this study, we collect data by exciting the mixed platoon system with small control inputs to the CAV, attack inputs to the CAV, and disturbances to the head vehicle. From the parametric model of the mixed platoon system (7), it can be found that the state $x(k)$ is affected by the control input $u(k)$, head vehicle's velocity disturbance $\epsilon(k)$, the attack $\vartheta(k)$, and the noise $\omega(k)$. Note that during data collection, $u(k), \epsilon(k), \vartheta(k), x(k)$ are all measurable, while $\omega(k)$ is unknown but bounded. This paper applies a sequence of persistently exciting inputs $u(k), \epsilon(k)$, and $\vartheta(k)$ with a length $T+1$ to the mixed platoon system for data collection. Specifically, the control input sequence U , the disturbance input sequence E , the attack input sequence F , and the corresponding state sequence X are defined as follows:

$$U = [u(1), u(2), \dots, u(T+1)] \in \mathbb{R}^{1 \times (T+1)}, \quad (10a)$$

$$E = [\epsilon(1), \epsilon(2), \dots, \epsilon(T+1)] \in \mathbb{R}^{1 \times (T+1)}, \quad (10b)$$

$$F = [\vartheta(1), \vartheta(2), \dots, \vartheta(T+1)] \in \mathbb{R}^{1 \times (T+1)}, \quad (10c)$$

$$X = [x(1), x(2), \dots, x(T+1)] \in \mathbb{R}^{2n \times (T+1)}. \quad (10d)$$

These data are all measurable, and will be processed into standardized formats to construct matrix zonotope set \mathcal{M}_{ABHJ} for reachable set computation and Hankel matrices for future trajectory predictions, respectively, as shown in Fig. 2. Particularly, for constructing matrix zonotope set \mathcal{M}_{ABHJ} , the data sequences are further reorganized as:

$$U_- = [u(1), u(2), \dots, u(T)] \in \mathbb{R}^{1 \times T}, \quad (11a)$$

$$E_- = [\epsilon(1), \epsilon(2), \dots, \epsilon(T)] \in \mathbb{R}^{1 \times T}, \quad (11b)$$

$$F_- = [\vartheta(1), \vartheta(2), \dots, \vartheta(T)] \in \mathbb{R}^{1 \times T}, \quad (11c)$$

$$X_- = [x(1), x(2), \dots, x(T)] \in \mathbb{R}^{2n \times T}, \quad (11d)$$

$$X_+ = [x(2), x(3), \dots, x(T+1)] \in \mathbb{R}^{2n \times T}. \quad (11e)$$

In addition, the sequence of unknown noise is denoted as

$$W_- = [\omega(1), \omega(2), \dots, \omega(T)] \in \mathbb{R}^{2n \times T}, \quad (12)$$

although it is important to note that W_- is not measurable. This notation is introduced solely to facilitate the proof of Lemma 1, and does not imply that W_- is measurable.

For constructing Hankel matrices in future trajectory predictions, we reformulate the trajectory data U_- , E_- , F_- , and X_- into a compact form as the following column vectors:

$$U_d = \text{col}(U_-) \in \mathbb{R}^T, \quad (13a)$$

$$E_d = \text{col}(E_-) \in \mathbb{R}^T, \quad (13b)$$

$$F_d = \text{col}(F_-) \in \mathbb{R}^T, \quad (13c)$$

$$X_d = \text{col}(X_-) \in \mathbb{R}^{2nT}. \quad (13d)$$

Remark 4: In this paper, the noise $\omega(k)$ in (12) is assumed to be bounded but not measurable. The disturbance $\epsilon(k)$ in (11b) is the velocity deviation of the head vehicle from its equilibrium state. Since the velocity of the head vehicle is directly measurable and its equilibrium state can be estimated, $\epsilon(k)$ can be explicitly determined. Finally, the historical attack $\vartheta(k)$ in (11c) is also reconstructible. This is because the control input issued by the cloud control platform is known, while the system input received by the CAV is also known and transmitted back to the cloud. By taking the difference between these two signals, the $\vartheta(k)$ in historical time steps can be obtained.

B. Offline Learning

In the offline learning phase, given that the matrices A , B , H , and J in (7) are unknown, we utilize pre-collected data to construct an over-approximated system matrix set \mathcal{M}_{ABHJ} . This set models the unknown and uncertain dynamics of the mixed platoon system. We then derive a data-driven stabilizing feedback control law K from data to ensure stability across all possible systems configurations represented by $[A \ B]$. Additionally, the Hankel matrices are formed using the pre-collected data and serve as part of the predictor. These components, the over-approximated system matrix set \mathcal{M}_{ABHJ} , the stabilizing feedback control law K , and the Hankel matrices, are later integral to the online control phase, discussed in Section III-C.

1) *Over-Approximated System Matrix Set:* We first construct the matrix zonotope set \mathcal{M}_{ABHJ} to over-approximate all possible system models $[A \ B \ H \ J]$ that are consistent with the noisy data. The following Lemma 1 is needed.

Lemma 1: Given the data sequences U_- , E_- , F_- , X_- , and X_+ from the mixed platoon system (7), and transforming the bounded forms of the disturbance $\epsilon(k)$, the attack $\vartheta(k)$, and the noise $\omega(k)$ in (8) to be zonotope sets, given by:

$$\begin{cases} \epsilon(k) \in \mathcal{Z}_\epsilon = \langle c_{\mathcal{Z}_\epsilon}, G_{\mathcal{Z}_\epsilon} \rangle = \langle 0, \epsilon_{\max} \rangle, \\ \vartheta(k) \in \mathcal{Z}_\vartheta = \langle c_{\mathcal{Z}_\vartheta}, G_{\mathcal{Z}_\vartheta} \rangle = \langle 0, \vartheta_{\max} \rangle, \\ \omega(k) \in \mathcal{Z}_\omega = \langle c_{\mathcal{Z}_\omega}, G_{\mathcal{Z}_\omega} \rangle = \langle \mathbf{0}_{2n \times 1}, \omega_{\max} \mathbf{I}_{2n \times 2n} \rangle, \end{cases} \quad (14)$$

where $\mathbf{0}$ and \mathbf{I} denote the zero and identity matrices of appropriate dimensions, respectively.

If the matrix $[X_-^\top \ U_-^\top \ E_-^\top \ F_-^\top]^\top$ is of full row rank, then the set of all possible $[A \ B \ H \ J]$ can be obtained:

$$\mathcal{M}_{ABHJ} = (X_+ - \mathcal{M}_\omega) \begin{bmatrix} X_- \\ U_- \\ E_- \\ F_- \end{bmatrix}^\dagger, \quad (15)$$

where \dagger is the Moore–Penrose pseudoinverse. The term \mathcal{M}_ω represents the noise matrix zonotope set:

$$\mathcal{M}_\omega = \left\langle C_{\mathcal{M}_\omega}, [G_{\mathcal{M}_\omega}^{(1)}, G_{\mathcal{M}_\omega}^{(2)}, \dots, G_{\mathcal{M}_\omega}^{(2nT)}] \right\rangle, \quad (16)$$

which is derived from the noise zonotope $\mathcal{Z}_\omega = \langle c_{\mathcal{Z}_\omega}, G_{\mathcal{Z}_\omega} \rangle$ in (14), with the specific formulations given as

$$C_{\mathcal{M}_\omega} = [c_{\mathcal{Z}_\omega} \ \dots \ c_{\mathcal{Z}_\omega}] \in \mathbb{R}^{2n \times T}, \quad (17a)$$

$$G_{\mathcal{M}_\omega}^{(1+(i-1)T)} = [g_{\mathcal{Z}_\omega}^{(i)} \ \mathbf{0}_{2n \times (T-1)}] \in \mathbb{R}^{2n \times T}, \quad (17b)$$

$$G_{\mathcal{M}_\omega}^{(j+(i-1)T)} = [\mathbf{0}_{2n \times (j-1)} \ g_{\mathcal{Z}_\omega}^{(i)} \ \mathbf{0}_{2n \times (T-j)}] \in \mathbb{R}^{2n \times T}, \quad (17c)$$

$$G_{\mathcal{M}_\omega}^{(T+(i-1)T)} = [\mathbf{0}_{2n \times (T-1)} \ g_{\mathcal{Z}_\omega}^{(i)}] \in \mathbb{R}^{2n \times T}, \quad (17d)$$

where $g_{\mathcal{Z}_\omega}^{(i)}$ denotes the i -th column of $G_{\mathcal{Z}_\omega}$ in (14), with $\forall i = \{1, 2, \dots, 2n\}$, and $j = \{2, 3, \dots, T-1\}$.

Proof: For the system description in (7), we have

$$X_+ = [A \ B \ H \ J] \begin{bmatrix} X_- \\ U_- \\ E_- \\ F_- \end{bmatrix} + W_-. \quad (18)$$

Since the matrix $[X_-^\top \ U_-^\top \ E_-^\top \ F_-^\top]^\top$ is of full row rank, then we could get

$$[A \ B \ H \ J] = (X_+ - W_-) \begin{bmatrix} X_- \\ U_- \\ E_- \\ F_- \end{bmatrix}^\dagger, \quad (19)$$

where the noise W_- in the collected data is unknown, but one can use the corresponding bounds \mathcal{M}_ω to obtain (15). Then, the matrix zonotope set \mathcal{M}_{ABHJ} is an over-approximation for system models $[A \ B \ H \ J]$ considering noisy data. ■

2) *Data-Driven Stabilizing Feedback Control Law*: We then aim to stabilize all possible $[A \ B]$ by a feedback law K . Collect data under the condition that $\epsilon(k) = 0$ and $\vartheta(k) = 0$, which are straightforward to achieve. Inspired by [63], we assume the data sequence W_- satisfies a quadratic matrix inequality:

$$\begin{bmatrix} I \\ W_- \end{bmatrix}^\top \Phi \begin{bmatrix} I \\ W_- \end{bmatrix} \geq 0, \quad (20)$$

where $\Phi = \begin{bmatrix} \Phi_{11} & \Phi_{12} \\ \Phi_{21} & \Phi_{22} \end{bmatrix} \in \mathbb{S}^{2n+T}$, with $\Phi_{11} \in \mathbb{S}^{2n}$, $\Phi_{12} \in \mathbb{R}^{2n \times T}$, $\Phi_{21} \in \mathbb{R}^{T \times 2n}$, $\Phi_{22} \in \mathbb{S}^T$. Based on the bound of $\omega(k)$ in W_- as described in (8), where $\|\omega(k)\|_\infty \leq \omega_{\max}$, we set $\Phi_{22} = -I$, $\Phi_{12} = 0$, and $\Phi_{11} = \omega_{\max}^2 T I$.

Then, the feedback control law K that stabilizes all possible systems $[A \ B]$ can be obtained by Lemma 2.

Lemma 2: For mixed platoon systems (7), if the assumption in (20) hold and the matrix $[X_-^\top \ U_-^\top]^\top$ is of full row rank, one can solve the following linear matrix inequalities (LMIs):

$$\begin{bmatrix} P & 0 \\ 0 & -P \end{bmatrix} - \begin{bmatrix} I & X_+ \\ 0 & -X_- \end{bmatrix} \Phi \begin{bmatrix} I & X_+ \\ 0 & -X_- \end{bmatrix}^\top > 0, \quad (21a)$$

$$P - [I \ X_+] \Phi \begin{bmatrix} I \\ X_+^\top \end{bmatrix} + \Theta \begin{bmatrix} X_- \\ U_- \end{bmatrix}^\top \Psi \begin{bmatrix} X_- \\ U_- \end{bmatrix} \Theta^\top > 0, \quad (21b)$$

$$\Psi = \left(\begin{bmatrix} X_- \\ U_- \end{bmatrix} \Phi_{22} \begin{bmatrix} X_- \\ U_- \end{bmatrix}^\top \right)^{-1}, \quad (21c)$$

to obtain the positive definite matrix P , where $\Theta = \Phi_{12} + X_+ \Phi_{22}$. Using P , the feedback gain can be obtained by

$$K = (U_- (\Phi_{22} + \Theta^\top \Gamma^\dagger \Theta) X_-^\top) (X_- (\Phi_{22} + \Theta^\top \Gamma^\dagger \Theta) X_-^\top)^\dagger, \quad (22)$$

which stabilizes all possible systems $[A \ B]$, where

$$\Gamma = P - [I \ X_+] \Phi \begin{bmatrix} I \\ X_+^\top \end{bmatrix}. \quad (23)$$

Proof: Lemma 2 is derived from [63, Theorem 5.3], with a detailed proof available in [63]. ■

3) *Hankel Matrices*: We finally utilize the pre-collected data U_d , E_d , F_d , X_d to form the Hankel matrices, which constitute part of the data-driven model used during online control in Section III-B. In particular, these matrices are partitioned into two parts, corresponding to the trajectory data in the past $T_{\text{ini}} \in \mathbb{N}$ steps and the trajectory data in the future $N \in \mathbb{N}$ steps, defined as follows:

$$\begin{aligned} \begin{bmatrix} U_p \\ U_f \end{bmatrix} &= \mathcal{H}_L(U_d), \quad \begin{bmatrix} E_p \\ E_f \end{bmatrix} = \mathcal{H}_L(E_d), \\ \begin{bmatrix} F_p \\ F_f \end{bmatrix} &= \mathcal{H}_L(F_d), \quad \begin{bmatrix} X_p \\ X_f \end{bmatrix} = \mathcal{H}_L(X_d), \end{aligned} \quad (24)$$

where $L = T_{\text{ini}} + N$, and U_p, U_f contain the upper T_{ini} rows and lower N rows of $\mathcal{H}_L(U_d)$, respectively (similarly for E_p and E_f , F_p and F_f , X_p and X_f).

Remark 5: Note that for the persistently exciting requirement of order $T_{\text{ini}} + N$, one sufficient condition is $T \geq 2(T_{\text{ini}} + N + 2n) - 1$ [39], [43]. This ensures that the input sequences U_- , E_- , and F_- are sufficiently long to excite the system fully. The generated state sequence X_- could capture the dynamic behavior of the mixed platoon under the influence of multi-source inputs.

C. Online Control

To ensure the robustness of the mixed platoon control system under noise and attacks, the reachable set technique is introduced. Inspired by the tube-based control method [64] and reach-avoid control method [57], the system is first decoupled into a nominal system and an error system. The reachable set of the error system is computed under disturbances, attacks, and noise. Then, the reachable set of the nominal system is obtained by subtracting the error reachable set from the practical constraints. Using these compact nominal constraints, the nominal control input is computed via the standard DeeP-LCC. Finally, the actual control input for the CAV is obtained by combining the nominal control input with the error feedback control input.

1) *Mixed Platoon System Decoupling*: We start by employing the parametric system model (7) to illustrate the decoupling process. The decoupled nominal system and the error system are denoted as follows:

$$x_z(k+1) = Ax_z(k) + Bu_z(k) + H\epsilon_z(k) + J\vartheta_z(k), \quad (25a)$$

$$x_e(k+1) = Ax_e(k) + Bu_e(k) + H\epsilon_e(k) + J\vartheta_e(k) + \omega(k), \quad (25b)$$

where $x_z(k)$, $u_z(k)$, $\epsilon_z(k)$, $\vartheta_z(k)$ and $x_e(k)$, $u_e(k)$, $\epsilon_e(k)$, $\vartheta_e(k)$ represent the state, control input, disturbance input, and attack input of the nominal dynamics system and error dynamics system, respectively. Specifically, we have

$$\begin{cases} x(k) = x_z(k) + x_e(k), \\ u(k) = u_z(k) + u_e(k), \\ \epsilon(k) = \epsilon_z(k) + \epsilon_e(k), \\ \vartheta(k) = \vartheta_z(k) + \vartheta_e(k). \end{cases} \quad (26)$$

Particularly, we set

$$\epsilon_z(k) = 0, \quad \epsilon_e(k) = \epsilon(k), \quad \vartheta_z(k) = 0, \quad \vartheta_e(k) = \vartheta(k), \quad (27)$$

so that the disturbance $\epsilon(k)$, the attack $\vartheta(k)$, and the noise $\omega(k)$ are considered exclusively in the error system, without affecting the nominal system. This simplifies the solution of the RDDeP-LCC optimization formulation in the following.

2) *Data-Driven Reachable Set of Error State*: Based on the noise, disturbance, and attack zonotope sets defined in (14), the model matrix zonotope set $\mathcal{M}_{\text{ABHJ}}$ derived in (15), and linear state feedback gain K derived in (22), we can compute the error state reachable set using Lemma 3 for the error dynamics described in (25b).

Lemma 3: For the system described by (25b), given input-state trajectories U_- , E_- , F_- , X_- , X_+ , if the matrix $[X_-^\top \ U_-^\top \ E_-^\top \ F_-^\top]^\top$ is of full row rank, then the recursive

relation for the data-driven error state reachable set can be computed as follows:

$$\hat{\mathcal{R}}_{k+i+1}^e = \mathcal{M}_{ABHJ} \left(\hat{\mathcal{R}}_{k+i}^e \times K \hat{\mathcal{R}}_{k+i}^e \times \mathcal{Z}_\epsilon \times \mathcal{Z}_\vartheta \right) + \mathcal{Z}_\omega, \quad (28)$$

where $\hat{\mathcal{R}}_{k+i}^e$ represents an over-approximated reachable set for the state $x_e(k+i)$ of the error dynamics system (25b).

Proof: From the error dynamics system (25b), the error state reachable set can be computed using the model:

$$\mathcal{R}_{k+i+1}^e = [A \ B \ H \ J] \left(\mathcal{R}_{k+i}^e \times K \mathcal{R}_{k+i}^e \times \mathcal{Z}_\epsilon \times \mathcal{Z}_\vartheta \right) + \mathcal{Z}_\omega. \quad (29)$$

Since $[A \ B \ H \ J] \in \mathcal{M}_{ABHJ}$, according to Lemma 1, and if \mathcal{R}_{k+i}^e and $\hat{\mathcal{R}}_{k+i}^e$ start from the same initial set, it is evident that $\mathcal{R}_{k+i+1}^e \in \hat{\mathcal{R}}_{k+i+1}^e$. Therefore, the recursive relation (28) holds, providing an over-approximated reachable set for the data-driven error state. ■

3) *RDdeP-LCC Optimization Formulation:* In this part, we proceed to design the RDdeP-LCC optimization formulation, which is extended from DeeP-LCC [39], for the mixed platoon to achieve optimal and safe control under disturbance $\epsilon(k)$, attacks $\vartheta(k)$, and noise $\omega(k)$.

a) *Trajectory Definition:* At each time step k , we define the state trajectory x_{ini} over the past T_{ini} steps and the future state trajectory x_z of the nominal system in the next N steps as follows:

$$\begin{cases} x_{\text{ini}} &= \text{col}(x(k - T_{\text{ini}}), x(k - T_{\text{ini}} + 1), \dots, x(k - 1)), \\ x_z &= \text{col}(x_z(k), x_z(k + 1), \dots, x_z(k + N - 1)). \end{cases} \quad (30)$$

The control trajectories u_{ini} and u_z , the disturbance trajectories ϵ_{ini} and ϵ_z , and the attack trajectories ϑ_{ini} and ϑ_z in the past T_{ini} steps and future N steps are defined similarly as in (30).

b) *Cost Function:* Similarly to DeeP-LCC [39], we utilize the quadratic function $J(x_z, u_z)$ to quantify the control performance by penalizing the states x_z and control inputs u_z of the nominal system (25a), defined as follows:

$$J(x_z, u_z) = \sum_{i=0}^{N-1} (\|x_z(k+i)\|_Q^2 + \|u_z(k+i)\|_R^2), \quad (31)$$

where $Q = \text{diag}(Q_x, \xi Q_x, \dots, \xi^{(n-1)} Q_x) \in \mathbb{R}^{2n \times 2n}$ and $R \in \mathbb{R}$ are the weight matrices penalizing the system states and control inputs, with $0 < \xi \leq 1$ denotes the decay factor. Precisely, we have $Q_x = \text{diag}(\rho_s, \rho_v)$, with ρ_s and ρ_v denoting the penalty weights for spacing deviation and velocity deviation, respectively.

c) *Constraints:* The safety of the mixed platoon system is ensured by imposing the following constraints:

$$\begin{cases} x(k+i) \in \mathcal{X}, \\ u(k+i) \in \mathcal{U}, \end{cases} \quad (32)$$

where $\mathcal{X} = \{x(k) \in \mathbb{R}^{2n} \mid |x(k)| \leq \mathbf{1}_n \otimes x_{\text{max}}\}$ is the state constraint, with $x_{\text{max}} = [\tilde{s}_{\text{max}}, \tilde{v}_{\text{max}}]^\top$, where \tilde{s}_{max} and \tilde{v}_{max} are the constraint limits for spacing deviation and velocity deviation, respectively. For the control input constraint, we define $\mathcal{U} = \{u(k) \in \mathbb{R} \mid |u(k)| \leq u_{\text{max}}\}$, where u_{max} denotes the maximum control input for the CAVs.

Combining (28) and (32), the constraint set for the nominal system (25a) can be calculated as follows:

$$\begin{cases} \mathcal{X}_z(k+i) = \mathcal{X} - \hat{\mathcal{R}}_{k+i}^e, \\ \mathcal{U}_z(k+i) = \mathcal{U} - K \hat{\mathcal{R}}_{k+i}^e, \end{cases} \quad (33)$$

which yields the constraints for the predicted trajectory of the nominal system (25a), given by:

$$\begin{cases} x_z(k+i) \in \mathcal{X}_z(k+i), \\ u_z(k+i) \in \mathcal{U}_z(k+i). \end{cases} \quad (34)$$

For the future disturbance sequence ϵ_z and attack sequence ϑ_z of the nominal system, recalling (27), we have

$$\epsilon_z(k+i) = 0, \quad \vartheta_z(k+i) = 0. \quad (35)$$

d) *Data-Driven Dynamics:* Based on Willems' fundamental lemma in [43, Theorem 1], [39, Proposition 2], and [42, Lemma 4.2], the data-driven dynamics of the mixed platoon system can be given by

$$\begin{bmatrix} X_p \\ U_p \\ E_p \\ F_p \\ X_f \\ U_f \\ E_f \\ F_f \end{bmatrix} g = \begin{bmatrix} x_{\text{ini}} \\ u_{\text{ini}} \\ \epsilon_{\text{ini}} \\ \vartheta_{\text{ini}} \\ x_z \\ u_z \\ \epsilon_z \\ \vartheta_z \end{bmatrix} + \begin{bmatrix} \sigma \\ 0 \\ 0 \\ 0 \\ 0 \\ 0 \\ 0 \\ 0 \end{bmatrix}, \quad (36)$$

where $\sigma \in \mathbb{R}^{2nT_{\text{ini}}}$ is a slack variable ensuring feasibility. The existence of $g \in \mathbb{R}^{T-T_{\text{ini}}-N+1}$ satisfying (36) implies that x_z , u_z , ϵ_z , and ϑ_z form a future trajectory of length N .

e) *RDdeP-LCC Optimization Problem:* Naturally, we could formulate the optimization problem to solve the control input for the CAVs in mixed platoon systems as follows:

$$\begin{aligned} \min_{g, u_z, x_z, \sigma} & J(x_z, u_z) + \lambda_g \|g\|_2^2 + \lambda_\sigma \|\sigma\|_2^2 \\ \text{s.t.} & (34), (35), (36), \end{aligned} \quad (37)$$

where λ_g and λ_σ denote the regularization penalty coefficients for the weighted two-norm for g and σ , respectively.

Solving (37) yields an optimal control sequence u_z and the predicted state sequence x_z of the nominal system. Then, by

$$u(k) = u_z(k) + K(x(k) - x_z(k)), \quad (38)$$

we obtain the control input for the CAV, where $x(k)$ is measured from the actual system, and K from (22).

For each time step k of the online data-driven predictive control, we solve the final RDdeP-LCC optimization problem (37) using the receding horizon technique. The detailed procedure of RDdeP-LCC is presented in Algorithm 1.

Remark 6: It is worth noting that in (37), x_{ini} , u_{ini} , ϵ_{ini} , ϑ_{ini} represent the past trajectories of the actual system (7), while x_z , u_z , ϵ_z , ϑ_z denote the predicted trajectories of the nominal system (25a). As shown in (27), we assume $\epsilon_z(k) = 0$ and $\vartheta_z(k) = 0$, and capture the actual disturbances $\epsilon_e(k) = \epsilon(k)$ and actual attacks $\vartheta_e(k) = \vartheta(k)$ solely in the error system (25b). Provided $\epsilon(k) \in \mathcal{Z}_\epsilon$ and $\vartheta(k) \in \mathcal{Z}_\vartheta$ in (14), the

Algorithm 1: RDDeP-LCC

Input: Pre-collected data (U, E, F, X) , constraints $(\mathcal{X}, \mathcal{U})$, weight (Q, R) , bounded \mathcal{Z}_ϵ , \mathcal{Z}_θ , and \mathcal{Z}_ω , past horizon T_{ini} , control horizon N , total number of steps N_f .

- 1 Construct data $(U_-, E_-, F_-, X_-, X_+)$ and data (U_d, E_d, F_d, X_d) ;
- 2 Offline construct Hankel matrices $U_p, U_f, E_p, E_f, F_p, F_f, X_p, X_f$ using (24), the matrix zonotope set $\mathcal{M}_{\text{ABHJ}}$ using (15), and the feedback control law K using (28) ;
- 3 Initialize past mixed platoon data $(x_{\text{ini}}, u_{\text{ini}}, \epsilon_{\text{ini}}, \vartheta_{\text{ini}})$ at the initial time step 0;
- 4 **while** $0 \leq k \leq N_f$ **do**
- 5 Compute data-driven error reachable sets to obtain $\hat{\mathcal{R}}_{k+i}^e$ using (28);
- 6 Compute constraint set for the nominal system to obtain $\mathcal{X}_z(k+i)$ and $\mathcal{U}_z(k+i)$ using (33);
- 7 Solve (37) to obtain the optimal control input sequence u_z and the state sequence x_z for the nominal system ;
- 8 Measure the actual state $x(k)$ from the actual system;
- 9 Obtain $u(k)$ from (38) and apply it as the control input to the CAV;
- 10 $k \leftarrow k + 1$ and update past mixed platoon data $(x_{\text{ini}}, u_{\text{ini}}, \epsilon_{\text{ini}}, \vartheta_{\text{ini}})$;
- 11 **end**

effects of disturbances and attacks are further incorporated into the calculation of the error reachable set (28), resulting in a more stringent constraint (34) on x_z and u_z of the nominal system. This approach addresses the influence of unknown future disturbances and attacks, which are often oversimplified as zero in previous research [39], [45], [46].

IV. NUMERICAL SIMULATION

In this section, we conduct numerical simulations to evaluate the effectiveness of the proposed RDDeP-LCC method for mixed platoons in the presence of noise and attacks.

A. Simulation Setup

For the simulations, we consider the mixed platoon configuration depicted in Fig. 1, setting the platoon size to $n = 3$. We model the dynamics of CAVs using (3), while the specific dynamics of HDVs are captured by the nonlinear OVM model [26], given by:

$$u_i(t) = \alpha_i (V(s_i(t)) - v_i) + \beta_i (v_{i-1}(t) - v_i(t)), \quad (39)$$

where α_i and β_i denote the driver's sensitivity parameters. The desired velocity $V(s_i(t))$ is defined as follows:

$$V(s_i(t)) = \begin{cases} 0, & s_i(t) \leq s_{\min} \\ f_v(s_i(t)), & s_{\min} < s_i(t) < s_{\max} \\ v_{\max}, & s_i(t) \geq s_{\max}, \end{cases} \quad (40)$$

where v_{\max} is the maximum velocity, and s_{\max} and s_{\min} denote the maximum and minimum spacing, respectively. Referencing [15], the nonlinear expression for $f_v(s_i(t))$ is given as follows:

$$f_v(s_i(t)) = \frac{v_{\max}}{2} \left(1 - \cos \left(\pi \frac{s_i(t) - s_{\min}}{s_{\max} - s_{\min}} \right) \right). \quad (41)$$

It is important to note that these models are solely used for state updates of the vehicles in the simulations, and are not integrated into the proposed data-driven control scheme. The parameters for HDVs are set as $\alpha_i = 0.6$, $\beta_i = 0.9$, $v_{\max} = 36 \text{ m/s}$, $s_{\max} = 35 \text{ m}$, and $s_{\min} = 5 \text{ m}$ in (39)-(41). The simulation parameters for the RDDeP-LCC are specified as follows:

- For data collection phase, around the equilibrium velocity of $v^* = 18 \text{ m/s}$, we generate random control inputs of the CAV by $u(t) \sim \mathbb{U}[-0.2, 0.2]$, random disturbance inputs for the head vehicle's velocity by $\epsilon(t) \sim \mathbb{U}[-0.5, 0.5]$, and random attack inputs by $\vartheta(t) \sim \mathbb{U}[-0.3, 0.3]$, where \mathbb{U} represents uniform distribution. The offline collected trajectories, with a length of $T = 600$ and a sampling interval of 0.05 s , are then employed to construct (10)-(13).
- For offline learning phase, based on these pre-collected data sequences, we derive the over-approximated system matrix set $\mathcal{M}_{\text{ABHJ}}$ using (15), compute the feedback control law K using (22) in Lemma 2, and construct the Hankel matrices using (24), satisfying the persistently exciting condition as discussed in [39], [43].
- For online control phase, the future sequence length is set to $N = 5$ and the past sequence length is chosen as $T_{\text{ini}} = 20$ for the state trajectory (30). The cost function (31) is configured with weight coefficients $\xi = 0.6$, $\rho_s = 0.5$, $\rho_v = 1$, and $R = 0.1$. Constraints are imposed as $x_{\max} = [7, 7]^T$ and $u_{\max} = 5$ in (32). In the optimization formulation (37), we use $\lambda_g = 10$ and $\lambda_\sigma = 10$. The simulation step length is $t_s = 0.05 \text{ s}$.

For comparison purposes, several baseline methods are considered: 1) the standard MPC method, which assumes full knowledge of system dynamics in (7); 2) the standard DeeP-LCC method from [39]; and 3) the ZPC method from [38], which utilizes zonotope sets for data-driven control, explicitly accounting for noise, disturbances, and attacks. All baseline methods share the same parameter values with RDDeP-LCC, except that standard MPC and standard DeeP-LCC use $N = 10$. Additionally, the standard DeeP-LCC and ZPC utilize the identical data sets with RDDeP-LCC. Furthermore, we also include an all-HDV scenario as a baseline, where the CAV is controlled using the OVM model in (39).

The simulations are performed utilizing MATLAB 2023a, with optimization problems solved via the *quadprog* solver. Reachable sets are computed using the CORA 2021 toolbox [65]. The simulations are deployed on a computer equipped with an Intel Core i9-13900KF CPU and 64 GB of RAM. To enhance computational efficiency, we employ the interval set defined in Definition 1 to over-approximate the zonotope set, as described in Definition 2, despite a slight

increase in the conservatism of the sets. The *interval* command is detailed in the CORA 2021 Manual [65].

B. Simulation Results

Standard test cycles are commonly used to evaluate mixed platoon control algorithms [38], [39], [46]. Inspired by the experiments conducted in [38], we utilize the Supplemental Federal Test Procedure for US06 (SFTP-US06) driving cycle as the velocity for the head vehicle, characterized by high-speed and high-acceleration driving behavior. This setup allows us to assess the effectiveness of the proposed RDDeP-LCC in enhancing platoon performance.

In the online control phase, the real-time velocity of the head vehicle is assumed to be the equilibrium velocity, resulting in zero disturbance input $\epsilon(k) = 0$. To examine the impact of noise and attack boundaries on control performance, we conduct simulations under various noise boundaries $\omega_{\max} \in \{0, 0.01, 0.02, 0.03, 0.04\}$ and attack boundaries $\vartheta_{\max} \in \{0, 1, 2, 3, 4\}$, based on localization requirements for local roads in the United States [66] and attack input ranges from [47].

The simulation results for RDDeP-LCC method and the baseline methods are depicted in Fig. 3. For brevity, we present the results under a noise boundary $\omega_{\max} = 0.02$ and an attack boundary $\vartheta_{\max} = 2$. As shown in Fig. 3(a)-(c), when all vehicles are HDVs, or when the CAV is controlled using standard DeeP-LCC or standard MPC, significant velocity error amplification occurs during rapid acceleration or deceleration of the head vehicle (around 10 s, 130 s, and 500 s–600 s). In contrast, as shown in Fig. 3(d)(e), velocity errors are notably reduced when the CAV employs ZPC or RDDeP-LCC. Notably, RDDeP-LCC achieves the most substantial reduction, demonstrating its effectiveness in mitigating the effects of noise and attacks.

It is important to note that different levels of noise and attack can significantly affect controller performance. To investigate sensitivity to these factors, we conduct 10 simulation tests for each combination of noise boundary ω_{\max} and attack boundary ϑ_{\max} . In order to quantify the performance of our method and other baseline methods under different noise boundaries ω_{\max} and attack boundaries ϑ_{\max} , we adopt the velocity mean absolute deviation R_v as a performance index for tracking, defined as follows:

$$R_v = \frac{1}{(t_f - t_0)} \frac{1}{n} \sum_{k=t_0}^{t_f} \sum_{i=1}^n |v_i(k) - v^*(k)|, \quad (42)$$

where t_0 and t_f are the start and end time steps, respectively.

In addition, based on (31), we apply the real cost value R_c obtained at each simulation under different control methods to quantify the control performance, expressed as follows:

$$R_c = \sum_{k=t_0}^{t_f} (\|x(k)\|_Q^2 + \|u(k)\|_R^2). \quad (43)$$

Fig. 4 presents the values of R_v and R_c for simulations conducted under different control methods. In Fig. 4(a), standard MPC, ZPC, and RDDeP-LCC exhibit smaller mean values

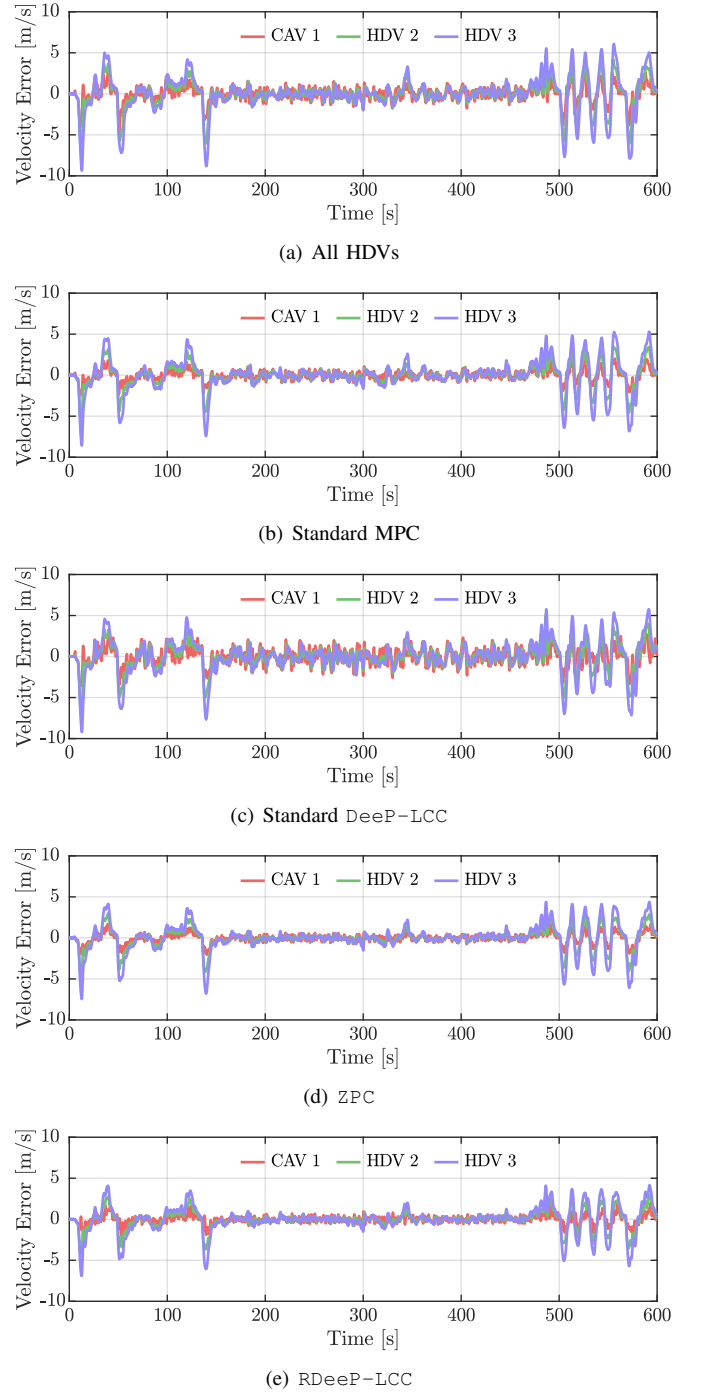


Fig. 3. Velocity errors in simulation results under five conditions: all vehicles are HDVs, standard MPC, standard DeeP-LCC, ZPC, and RDDeP-LCC. The red profiles represent the CAV (indexed as 1), the green profiles represent HDV (indexed as 2), and the purple profiles represent HDV (indexed as 3).

for R_v compared to all-HDV configuration across varying ω_{\max} and ϑ_{\max} conditions. Notably, RDDeP-LCC achieves the lowest mean R_v values. Higher values of R_v indicate greater velocity error, reflecting a reduced capability of the CAVs to track the head vehicle accurately. These results highlight the superiority of the proposed RDDeP-LCC method over standard MPC and ZPC in mixed platoon velocity tracking performance, significantly outperforming the all-HDV configuration. Although the overall control performance degrades as

the attack bound ϑ_{\max} increases, RDDeP-LCC consistently maintains a clear advantage over the baseline methods under various levels of adversarial attacks. It is noteworthy that for standard DeeP-LCC, R_v value is lower than that of all-HDV configuration only when approximately $\vartheta_{\max} \leq 0.5$. Under higher attack boundaries, the standard DeeP-LCC exhibits higher R_v values than all-HDV configuration, indicating its lack of robustness against noise and attacks without specific robust design.

Furthermore, Fig. 4(b) illustrates the real cost values R_c in (43) for our RDDeP-LCC method and baseline methods. The results clearly show that our RDDeP-LCC method consistently achieves the lowest cost values R_c values across different conditions. This advantage is due to our emphasis on noise and attack mitigation through reachability set analysis, which maintains tighter state constraints for the mixed platoon system, thus ensuring robustness in dynamic environments. While standard MPC shows lower R_c values than all HDVs, it lacks specific considerations for attack mitigation, resulting in higher R_c values compared to our method. The ZPC achieves comparable R_c values to RDDeP-LCC due to its use of reachable sets for robustness assurance. However, unlike RDDeP-LCC, which integrates both offline and online data for dynamics construction, ZPC relies solely on offline data. This reliance may limit model accuracy, leading to slightly higher R_c values compared to RDDeP-LCC. Notably, for the standard DeeP-LCC method, its R_c remains low when attacks are absent. However, as noise and attack increase, its performance becomes unacceptable, with the mean R_c value reaching 1.2×10^5 when $\vartheta_{\max} = 4$. This performance degradation is attributed to the heavy reliance of the standard DeeP-LCC on data for modeling (36), where the presence of data noise significantly reduces model accuracy. Additionally, standard DeeP-LCC lacks preemptive robustness against attacks, further compromising its control performance in environments with coexisting noise and attacks. In contrast, our proposed RDDeP-LCC method demonstrates enhanced robustness against noise and attacks, ensuring reliable mixed platoon control. By integrating reachability set analysis into the data-driven control framework, our method effectively addresses the challenges posed by noise and attacks.

To evaluate the computational efficiency of the proposed method, we analyze its offline and online phases. In the offline phase, constructing the over-approximated system matrix set \mathcal{M}_{ABHJ} in (15) requires 0.15 s, computing the data-driven stabilizing feedback control law K in (22) takes 0.65 s, and generating the Hankel matrices in (24) is completed within 0.03 s. Notably, \mathcal{M}_{ABHJ} is also used in ZPC, and the Hankel matrices are shared with DeeP-LCC, ensuring consistency across these methods. In the online phase, Table I summarizes the average computation time R_t for each method. The standard MPC exhibits the fastest execution time of 0.001 s. The ZPC requires a modest increase to 0.018 s due to the online computation of reachable sets. The DeeP-LCC requires 0.024 s, mainly attributed to solving an optimization problem with decision variable g of size $T - T_{\text{ini}} - N + 1$. Similarly, the proposed RDDeP-LCC takes 0.038 s. Notably, the online computation time of RDDeP-LCC remains within the 0.05 s

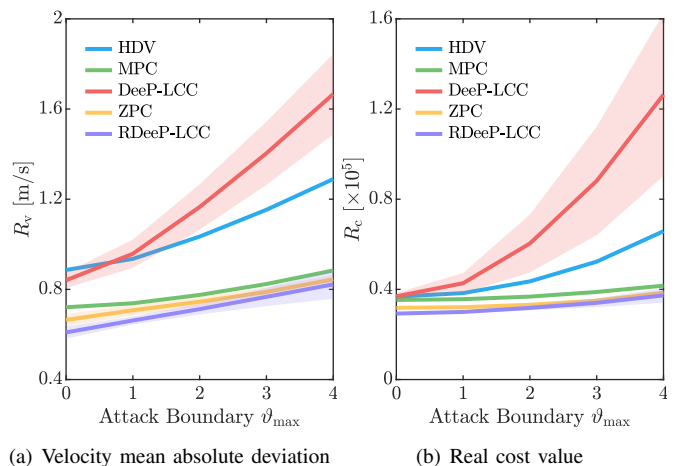


Fig. 4. The values of R_v and R_c for multiple simulations under different methods. The dark-colored solid lines represent the mean values of R_v and R_c across multiple simulations, and the light-colored shaded areas depict the mean \pm standard deviation.

TABLE I
COMPUTATIONAL TIME

	MPC	DeeP-LCC	ZPC	RDDeP-LCC
R_t (s)	0.001	0.024	0.018	0.038

sampling period, ensuring its real-time applicability without inducing control delay.

V. HUMAN-IN-THE-LOOP EXPERIMENT

In this section, we establish a human-in-the-loop bench experimental platform to verify the effectiveness of the RDDeP-LCC method proposed in this paper.

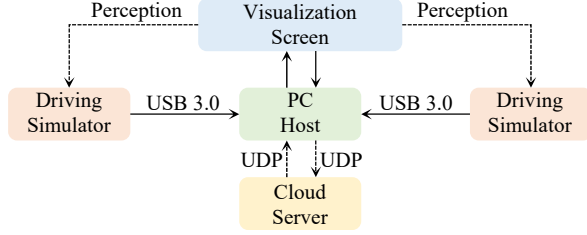
A. Human-in-the-Loop Experimental Platform

To validate the effectiveness of the RDDeP-LCC method under process noise and adversarial attacks, we developed a human-in-the-loop platform that replicates a real-world driving scenario using PreScan 8.5 software on a Windows 10 system. As depicted in Fig. 5, the setup comprises a visualization screen module, two Logitech G29 driving simulator modules (including brake pedal, accelerator pedal, and steering wheel), a PC host module equipped with an Intel Core i9-13900KF CPU and 64 GB of RAM, and a cloud server powered by an Intel(R) Xeon(R) Gold 6226R CPU @ 2.90GHz.

In this setup, the experiment is conducted on a straight road. Drivers observe the preceding vehicles through a high-definition visualization screen module and control their vehicles using the Logitech G29 driving simulators. These simulators are connected to the PC host module's Simulink software via the USB 3.0, enabling the real-time transmission of control commands from the drivers to Simulink, including braking and acceleration maneuvers. Subsequently, Simulink relays these commands to PreScan 8.5 software, which displays the vehicle dynamic in real-time on the visualization screen. The detailed dynamics model of the simulated vehicles is based on the Audi A8 model provided by PreScan 8.5. The control algorithm



(a) Experimental devices



(b) Connection structure

Fig. 5. Human-in-the-loop experimental platform for mixed platoon control.

is developed within the Matlab/Simulink environment and deployed on a cloud server. Vehicle states and control inputs are transmitted between the PC host and the cloud server using UDP communication. Additionally, to simulate realistic driving conditions, we use the *uniform random number* module in Simulink to simulate noise and attacks. The entire experiment operates at a simulation frequency of 20 Hz.

B. Experimental Design

Utilizing the human-in-the-loop platform, we conduct experimental validation of the RDeeP-LCC method and baseline methods. In our experiments, the RDeeP-LCC method or other baseline methods control the CAV (indexed as 1), while two drivers operate the HDVs (indexed as 2 and 3) using the Logitech G29 simulators. To ensure accuracy and consistency, before the formal experiment, drivers undergo a 3-hour training session in car-following scenarios to familiarize themselves with the driving simulators. Furthermore, to ensure fairness in the comparative experiment, all drivers are informed that the study involves mixed platoon control strategies. However, they are not informed of which specific control algorithm is implemented on the CAV, nor are they made aware of the evaluation metrics used in the analysis. Throughout the experiment, each driver is instructed to maintain their natural car-following behavior. To replicate a realistic traffic scenario, the head vehicle (indexed as 0) is assigned a time-varying velocity profile derived from the SFTP-US06 driving cycle, while subject to a noise boundary of $\omega_{\max} = 0.02$ and an attack boundary of $\vartheta_{\max} = 2$. All other experimental configurations are consistent with the simulation settings outlined in Section IV.

In this experiment, we initially set the velocity of the head vehicle as the equilibrium velocity v_i^* . It is important

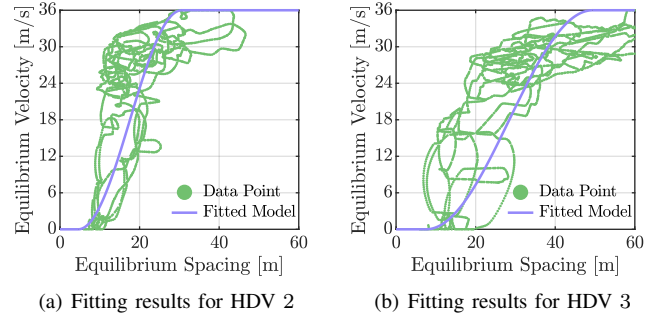


Fig. 6. The fitting results of equilibrium spacings and equilibrium velocities for the two HDVs. The green points represent the collected data, and the purple lines represent the relationship between equilibrium spacings and equilibrium velocities fitted using the OVM framework.

to note that unlike the OVM model (39) utilized by HDVs in Section IV, where equilibrium spacing s_i^* can be directly calculated from v_i^* based on (40) and (41) during the simulation. However, it is a challenge for us to get the equilibrium spacing s_i^* for real drives. To address this issue, we conduct a preliminary experiment where two drivers operate their vehicles in a car-following scenario using the SFTP-US06 driving cycle. Subsequently, we gather experimental data, represented by the green points in Fig. 6. This data is then utilized to fit the HDVs model using the OVM model (40) and (41) as the foundation for MPC. The fitting results for two drivers, namely HDV 2 and HDV 3, are illustrated by the purple lines in Fig. 6(a) and (b), respectively. The parameters obtained from the fitting process for the two drivers are as follows: for HDV 2, $v_{\max} = 36$ m/s, $s_{\min} = 4.6$ m, $s_{\max} = 30.6$ m; for HDV 3, $v_{\max} = 36$ m/s, $s_{\min} = 7.5$ m, $s_{\max} = 49.4$ m. By employing the fitted model, we are able to make estimations regarding the equilibrium spacing s_i^* in the online predictive control phase.

In the formal experiments for method validation, we first conduct data collection of the mixed platoon. The data collection settings are the same as in Section IV, except that real human drivers are used. In the offline phase, based on the collected data, we proceed with the construction of the matrix zonotope set \mathcal{M}_{ABHJ} in (15), the feedback control law K in (22), and the Hankel matrices in (24), as outlined in Section IV. Subsequently, we transition to the online predictive control phase. Here, the head vehicle initiates its motion according to the predefined profile, while the CAV and two HDVs respond to the controller's commands and the drivers' actions, respectively. Upon completion of the trial, experimental data are gathered for subsequent analysis. The settings for this phase align with those detailed in Section IV.

C. Experimental Results

The experimental results comparing the algorithm proposed in this study with other baseline methods are presented in Fig. 7. In the presence of noise and attacks, significant velocity tracking errors are observed in all HDVs, as illustrated in Fig. 7(a), indicating inadequate tracking performance for all HDV scenarios. Notably, the standard

DeeP-LCC method shows more pronounced velocity tracking errors than all HDVs, as depicted in Fig. 7(c). These errors stem from the DeeP-LCC method's lack of tailored approaches to address noise and attack issues. Specifically, noise disrupts the data-driven dynamics model, while attacks directly impact the CAV's dynamic behavior, resulting in decreased tracking accuracy. In contrast, standard MPC, ZPC, and RDeeP-LCC significantly improve the tracking performance of the mixed platoon. Furthermore, a comparison between Fig. 7(b), Fig. 7(d), and Fig. 7(e) reveals that the vehicles' tracking error in the RDeeP-LCC method is even smaller. This outcome underscores the exceptional tracking performance of the RDeeP-LCC method, highlighting its robustness and efficacy in achieving precise control under diverse traffic conditions.

To comprehensively evaluate vehicle performance under different control strategies, three experiments are conducted for each controller. In addition to R_v in (42) and R_c in (43), two additional performance metrics fuel consumption R_f and driving comfort R_a are introduced:

$$R_f = t_s \sum_{k=t_0}^{t_f} \sum_{i=1}^n f_i, \quad (44)$$

$$R_a = \frac{1}{(t_f - t_0)} \frac{1}{n} \sum_{k=t_0}^{t_f} \sum_{i=1}^n (a_i)^2, \quad (45)$$

where f_i (mL/s) represents the fuel consumption rate of vehicle i , computed using the model in [39], [67], and a_i denotes its acceleration.

Table II provides the performance of all controllers across the four evaluation metrics (R_v , R_c , R_f , R_a). The results clearly demonstrate that the proposed RDeeP-LCC method outperforms all baseline approaches in terms of R_v , R_c , R_f , and R_a . Specifically, compared with the all HDVs, the RDeeP-LCC achieves improvements of 26.1 %, 24.7 %, 11.4 %, and 26.0 % across the respective metrics, highlighting its superior control capability. Conversely, the standard MPC approach yields improvements of only 18.8 %, 16.5 %, 5.5 %, and 5.7 %, and ZPC achieves slightly better results with 24.2 %, 22.7 %, 9.7 %, and 24.5 % improvements, respectively. Notably, the standard DeeP-LCC method reports the highest values (i.e., the worst performance) for all four metrics. This outcome suggests that purely data-driven predictive control, without robust design mechanisms, may struggle to meet desired performance standards in the presence of noise and attacks. In fact, such approaches might even exhibit worse performance compared to the inherent capabilities of all HDVs. In contrast, our RDeeP-LCC approach focuses on optimizing constraints using reachable set analysis, seeking to ensure that the state of a mixed platoon system remains within a tighter set of safety constraints. By explicitly accounting for uncertainties during optimization, the proposed approach enhances tracking precision, control efficiency, energy economy, and driving comfort in mixed platoon control systems under noise and attacks.

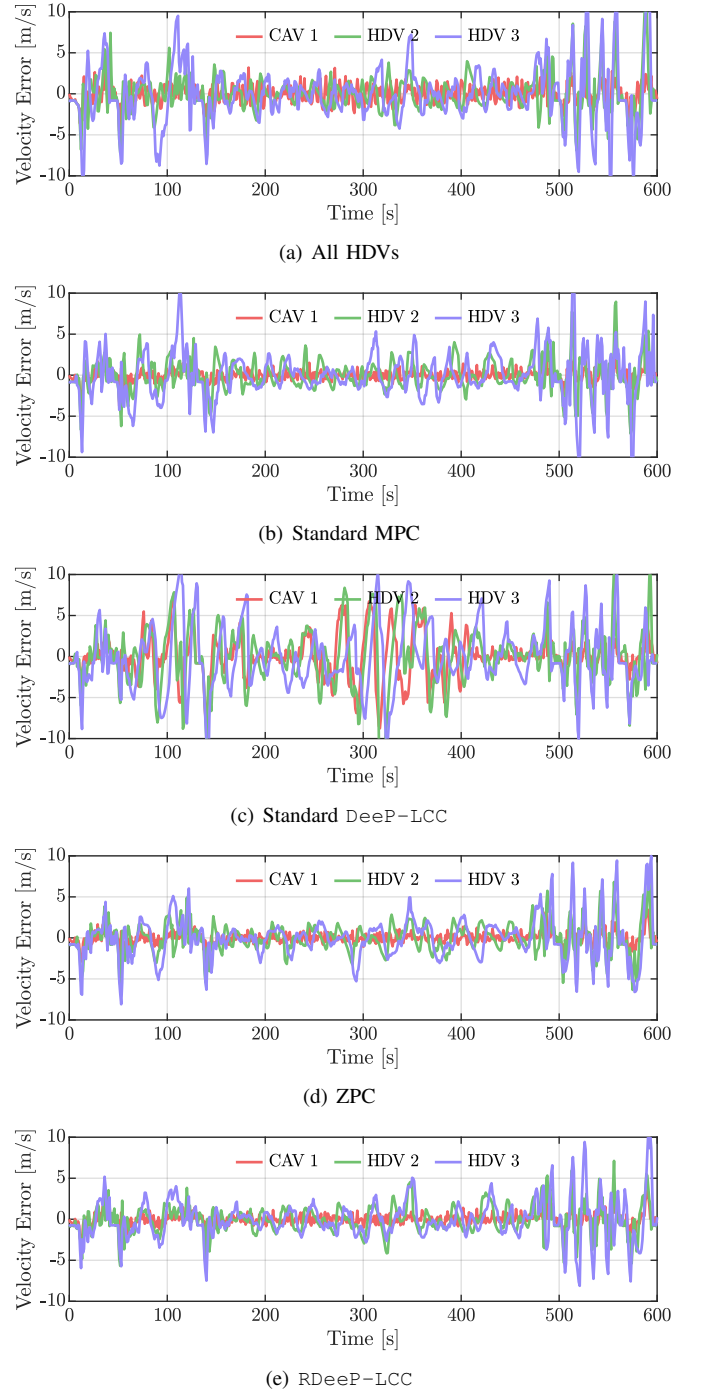


Fig. 7. Velocity errors in mixed platoon human-in-the-loop experimental under all vehicles are HDVs, standard MPC, standard DeeP-LCC, ZPC, and RDeeP-LCC. The red, green, and purple profiles represent the CAV (indexed as 1) and the HDVs (indexed as 2, 3), respectively.

VI. CONCLUSION

In this paper, we propose a novel RDeeP-LCC method for mixed platoon control under conditions of data noise and adversarial attacks. The RDeeP-LCC method incorporates the unknown dynamics for HDVs and directly relies on trajectory data of mixed platoons to construct data-driven reachable set constraints and a data-driven predictive controller, which provides safe and robust control inputs for CAVs. To vali-

TABLE II
PERFORMANCE INDICES IN HUMAN-IN-THE-LOOP EXPERIMENT

Index	R_v [m/s]	R_c [-]	R_f [mL]	R_a [m ² /s ⁴]
All HDVs	1.65 (— — —)	0.97×10^6 (— — —)	8133 (— — —)	3.88 (— — —)
MPC	1.34 (↓ 18.8 %)	0.81×10^6 (↓ 16.5 %)	7687 (↓ 5.5 %)	3.66 (↓ 5.7 %)
DeeP-LCC	2.40 (↑ 45.5 %)	3.53×10^6 (↑ 263.9 %)	8515 (↑ 4.7 %)	4.05 (↑ 4.4 %)
ZPC	1.25 (↓ 24.2 %)	0.75×10^6 (↓ 22.7 %)	7341 (↓ 9.7 %)	2.93 (↓ 24.5 %)
RDDeP-LCC	1.22 (↓ 26.1 %)	0.73×10^6 (↓ 24.7 %)	7205 (↓ 11.4 %)	2.87 (↓ 26.0 %)

date the effectiveness and superiority of this method, both numerical simulations and human-in-the-loop experiments are conducted. The results indicate that the RDDeP-LCC method has significantly improved the tracking performance of mixed platoons in the presence of data noise and adversarial attacks.

In future research, one practical concern in RDDeP-LCC is the influence of communication delays induced by actuators and communication. Existing studies have shown the potential of standard DeeP-LCC in addressing delay issues [68], but there is still a lack of customized data-driven control strategies. Another interesting topic is to improve the real-time computational efficiency of data-driven predictive control methods, which facilitates scalable deployment in real-world traffic scenarios. Furthermore, an important extension is to incorporate attack estimation techniques into the control framework, which can reduce conservatism and further improve system resilience.

REFERENCES

- [1] Z. Wang, G. Wu, and M. J. Barth, "A review on cooperative adaptive cruise control (cacc) systems: Architectures, controls, and applications," in *2018 21st International Conference on Intelligent Transportation Systems (ITSC)*. IEEE, 2018, pp. 2884–2891.
- [2] A. Alessandrini, F. Ortenzi, L. Berzi, M.-S. Gulino, F. Cignini, and L. Pugi, "An innovative convoying and power management system for public transportation," in *2023 IEEE 97th Vehicular Technology Conference (VTC2023-Spring)*. IEEE, 2023, pp. 1–5.
- [3] J. C. De Winter, R. Happee, M. H. Martens, and N. A. Stanton, "Effects of adaptive cruise control and highly automated driving on workload and situation awareness: A review of the empirical evidence," *Transportation Research Part F: Traffic Psychology and Behaviour*, vol. 27, pp. 196–217, 2014.
- [4] Y. Luo, T. Chen, S. Zhang, and K. Li, "Intelligent hybrid electric vehicle acc with coordinated control of tracking ability, fuel economy, and ride comfort," *IEEE Transactions on Intelligent Transportation Systems*, vol. 16, no. 4, pp. 2303–2308, 2015.
- [5] G. Gunter, D. Gloudemans, R. E. Stern, S. McQuade, R. Bhadani, M. Bunting, M. L. Delle Monache, R. Lysecky, B. Seibold, J. Sprinkle *et al.*, "Are commercially implemented adaptive cruise control systems string stable?" *IEEE Transactions on Intelligent Transportation Systems*, vol. 22, no. 11, pp. 6992–7003, 2020.
- [6] M. Makridis, K. Mattas, B. Ciuffo, F. Re, A. Kriston, F. Minarini, and G. Rognelund, "Empirical study on the properties of adaptive cruise control systems and their impact on traffic flow and string stability," *Transportation Research Record*, vol. 2674, no. 4, pp. 471–484, 2020.
- [7] M. Shen and G. Orosz, "Data-driven predictive connected cruise control," in *2023 IEEE Intelligent Vehicles Symposium (IV)*. IEEE, 2023, pp. 1–6.
- [8] J. Boo and D. Chwa, "Integral sliding mode control-based robust bidirectional platoon control of vehicles with the unknown acceleration and mismatched disturbance," *IEEE Transactions on Intelligent Transportation Systems*, vol. 24, no. 10, pp. 10881–10894, 2023.
- [9] S. Öncü, J. Ploeg, N. Van de Wouw, and H. Nijmeijer, "Cooperative adaptive cruise control: Network-aware analysis of string stability," *IEEE Transactions on Intelligent Transportation Systems*, vol. 15, no. 4, pp. 1527–1537, 2014.
- [10] S. W. Smith, Y. Kim, J. Guanetti, R. Li, R. Firoozi, B. Wootton, A. A. Kurzhanskiy, F. Borrelli, R. Horowitz, and M. Arcaç, "Improving urban traffic throughput with vehicle platooning: Theory and experiments," *IEEE Access*, vol. 8, pp. 141 208–141 223, 2020.
- [11] F. Ma, Y. Yang, J. Wang, Z. Liu, J. Li, J. Nie, Y. Shen, and L. Wu, "Predictive energy-saving optimization based on nonlinear model predictive control for cooperative connected vehicles platoon with v2v communication," *Energy*, vol. 189, p. 116120, 2019.
- [12] M. Tajalli and A. Hajbabaie, "Traffic signal timing and trajectory optimization in a mixed autonomy traffic stream," *IEEE Transactions on Intelligent Transportation Systems*, vol. 23, no. 7, pp. 6525–6538, 2021.
- [13] D. Hajdu, I. G. Jin, T. Insperger, and G. Orosz, "Robust design of connected cruise control among human-driven vehicles," *IEEE Transactions on Intelligent Transportation Systems*, vol. 21, no. 2, pp. 749–761, 2019.
- [14] Y. Jiang, F. Zhu, Z. Yao, Q. Gu, and B. Ran, "Platoon intensity of connected automated vehicles: definition, formulas, examples, and applications," *Journal of Advanced Transportation*, vol. 2023, no. 1, p. 3325530, 2023.
- [15] I. G. Jin and G. Orosz, "Optimal control of connected vehicle systems with communication delay and driver reaction time," *IEEE Transactions on Intelligent Transportation Systems*, vol. 18, no. 8, pp. 2056–2070, 2016.
- [16] C. Chen, J. Wang, Q. Xu, J. Wang, and K. Li, "Mixed platoon control of automated and human-driven vehicles at a signalized intersection: dynamical analysis and optimal control," *Transportation Research Part C: Emerging Technologies*, vol. 127, p. 103138, 2021.
- [17] J. Yang, D. Zhao, J. Lan, S. Xue, W. Zhao, D. Tian, Q. Zhou, and K. Song, "Eco-driving of general mixed platoons with cavs and hdvs," *IEEE Transactions on Intelligent Vehicles*, vol. 8, no. 2, pp. 1190–1203, 2022.
- [18] R. E. Stern, S. Cui, M. L. Delle Monache, R. Bhadani, M. Bunting, M. Churchill, N. Hamilton, H. Pohlmann, F. Wu, B. Piccoli *et al.*, "Dissipation of stop-and-go waves via control of autonomous vehicles: Field experiments," *Transportation Research Part C: Emerging Technologies*, vol. 89, pp. 205–221, 2018.
- [19] J. Wang, Y. Zheng, Q. Xu, J. Wang, and K. Li, "Controllability analysis and optimal control of mixed traffic flow with human-driven and autonomous vehicles," *IEEE Transactions on Intelligent Transportation Systems*, vol. 22, no. 12, pp. 7445–7459, 2020.
- [20] C. Wu, A. R. Kreidieh, K. Parvate, E. Vinitzky, and A. M. Bayen, "Flow: A modular learning framework for mixed autonomy traffic," *IEEE Transactions on Robotics*, vol. 38, no. 2, pp. 1270–1286, 2021.
- [21] J. Zhan, Z. Ma, and L. Zhang, "Data-driven modeling and distributed predictive control of mixed vehicle platoons," *IEEE Transactions on Intelligent Vehicles*, vol. 8, no. 1, pp. 572–582, 2022.
- [22] J. Guo, H. Guo, J. Liu, D. Cao, and H. Chen, "Distributed data-driven predictive control for hybrid connected vehicle platoons with guaranteed robustness and string stability," *IEEE Internet of Things Journal*, vol. 9, no. 17, pp. 16 308–16 321, 2022.
- [23] J. Wang, Y. Zheng, J. Dong, C. Chen, M. Cai, K. Li, and Q. Xu, "Implementation and experimental validation of data-driven predictive control for dissipating stop-and-go waves in mixed traffic," *IEEE Internet of Things Journal*, vol. 11, no. 3, pp. 4570–4585, 2023.
- [24] I. G. Jin, S. S. Avedisov, C. R. He, W. B. Qin, M. Sadeghpour, and G. Orosz, "Experimental validation of connected automated vehicle design among human-driven vehicles," *Transportation Research Part C: Emerging Technologies*, vol. 91, pp. 335–352, 2018.
- [25] M. Treiber, A. Hennecke, and D. Helbing, "Congested traffic states in empirical observations and microscopic simulations," *Physical Review E*, vol. 62, no. 2, p. 1805, 2000.

- [26] M. Bando, K. Hasebe, A. Nakayama, A. Shibata, and Y. Sugiyama, "Dynamical model of traffic congestion and numerical simulation," *Physical Review E*, vol. 51, no. 2, p. 1035, 1995.
- [27] S. Feng, Z. Song, Z. Li, Y. Zhang, and L. Li, "Robust platoon control in mixed traffic flow based on tube model predictive control," *IEEE Transactions on Intelligent Vehicles*, vol. 6, no. 4, pp. 711–722, 2021.
- [28] C. Liu, F. Zheng, R. Li, and X. Liu, "An anti-disturbance adaptive control approach for automated vehicles in mixed connected traffic environment," *IEEE Transactions on Intelligent Transportation Systems*, vol. 24, no. 12, pp. 15 274–15 287, 2023.
- [29] Y. Wang, S. Lin, Y. Wang, B. De Schutter, and J. Xu, "Robustness analysis of platoon control for mixed types of vehicles," *IEEE Transactions on Intelligent Transportation Systems*, vol. 24, no. 1, pp. 331–340, 2022.
- [30] C. Zhao, H. Yu, and T. G. Molnar, "Safety-critical traffic control by connected automated vehicles," *Transportation Research Part C: Emerging Technologies*, vol. 154, p. 104230, 2023.
- [31] W. Gao, Z.-P. Jiang, and K. Ozbay, "Data-driven adaptive optimal control of connected vehicles," *IEEE Transactions on Intelligent Transportation Systems*, vol. 18, no. 5, pp. 1122–1133, 2016.
- [32] M. Huang, Z.-P. Jiang, and K. Ozbay, "Learning-based adaptive optimal control for connected vehicles in mixed traffic: robustness to driver reaction time," *IEEE Transactions on Cybernetics*, vol. 52, no. 6, pp. 5267–5277, 2020.
- [33] E. Vinitsky, K. Parvate, A. Kreidieh, C. Wu, and A. Bayen, "Lagrangian control through deep-rl: Applications to bottleneck decongestion," in *2018 21st International Conference on Intelligent Transportation Systems (ITSC)*. IEEE, 2018, pp. 759–765.
- [34] J. Lan, D. Zhao, and D. Tian, "Safe and robust data-driven cooperative control policy for mixed vehicle platoons," *International Journal of Robust and Nonlinear Control*, vol. 33, no. 7, pp. 4171–4190, 2023.
- [35] J. Zhou, L. Yan, and K. Yang, "Safe reinforcement learning for mixed-autonomy platoon control," in *2023 IEEE 26th International Conference on Intelligent Transportation Systems (ITSC)*. IEEE, 2023, pp. 5744–5749.
- [36] —, "Enhancing system-level safety in mixed-autonomy platoon via safe reinforcement learning," *IEEE Transactions on Intelligent Vehicles*, pp. 1–13, 2024.
- [37] L. Hewing, K. P. Wabersich, M. Menner, and M. N. Zeilinger, "Learning-based model predictive control: Toward safe learning in control," *Annual Review of Control, Robotics, and Autonomous Systems*, vol. 3, pp. 269–296, 2020.
- [38] J. Lan, D. Zhao, and D. Tian, "Data-driven robust predictive control for mixed vehicle platoons using noisy measurement," *IEEE Transactions on Intelligent Transportation Systems*, vol. 24, no. 6, pp. 6586–6596, 2021.
- [39] J. Wang, Y. Zheng, K. Li, and Q. Xu, "Deep-lcc: Data-enabled predictive leading cruise control in mixed traffic flow," *IEEE Transactions on Control Systems Technology*, vol. 31, no. 6, pp. 2760–2776, 2023.
- [40] Y. Wu, Z. Zuo, Y. Wang, and Q. Han, "Driver-centric data-driven robust model predictive control for mixed vehicular platoon," *Nonlinear Dynamics*, vol. 111, no. 22, pp. 20 975–20 989, 2023.
- [41] H. Lyu, Y. Guo, P. Liu, Y. Wu, Q. Yue, and T. Wang, "Kooplcc: The koopman operator-based predictive leading cruise control for mixed vehicle platoons considering the driving styles," in *2024 IEEE 27th International Conference on Intelligent Transportation Systems (ITSC)*. IEEE, 2024, pp. 01–06.
- [42] J. Coulson, J. Lygeros, and F. Dörfler, "Data-enabled predictive control: In the shallows of the deepc," in *2019 18th European Control Conference (ECC)*. IEEE, 2019, pp. 307–312.
- [43] J. C. Willems, P. Rapisarda, I. Markovsky, and B. L. De Moor, "A note on persistency of excitation," *Systems & Control Letters*, vol. 54, no. 4, pp. 325–329, 2005.
- [44] J. Wang, Y. Zheng, C. Chen, Q. Xu, and K. Li, "Leading cruise control in mixed traffic flow: System modeling, controllability, and string stability," *IEEE Transactions on Intelligent Transportation Systems*, vol. 23, no. 8, pp. 12 861–12 876, 2021.
- [45] D. Li, K. Zhang, H. Dong, Q. Wang, Z. Li, and Z. Song, "Physics-augmented data-enabled predictive control for eco-driving of mixed traffic considering diverse human behaviors," *IEEE Transactions on Control Systems Technology*, vol. 32, no. 4, pp. 1479–1486, 2024.
- [46] K. Zhang, K. Chen, Z. Li, J. Chen, and Y. Zheng, "Privacy-preserving data-enabled predictive leading cruise control in mixed traffic," *IEEE Transactions on Intelligent Transportation Systems*, vol. 25, no. 5, pp. 3467–3482, 2023.
- [47] Q. Xu, Y. Liu, J. Pan, J. Wang, J. Wang, and K. Li, "Reachability analysis plus satisfiability modulo theories: An adversary-proof control method for connected and autonomous vehicles," *IEEE Transactions on Industrial Electronics*, vol. 70, no. 3, pp. 2982–2992, 2022.
- [48] C. Zhao and H. Yu, "Robust safety for mixed-autonomy traffic with delays and disturbances," *IEEE Transactions on Intelligent Transportation Systems*, vol. 25, no. 11, pp. 16 522 – 16 535, 2024.
- [49] L. Huang, J. Zhen, J. Lygeros, and F. Dörfler, "Robust data-enabled predictive control: Tractable formulations and performance guarantees," *IEEE Transactions on Automatic Control*, vol. 68, no. 5, pp. 3163–3170, 2023.
- [50] J. Berberich, J. Köhler, M. A. Müller, and F. Allgöwer, "Data-driven model predictive control with stability and robustness guarantees," *IEEE Transactions on Automatic Control*, vol. 66, no. 4, pp. 1702–1717, 2020.
- [51] X. Shang, J. Wang, and Y. Zheng, "Smoothing mixed traffic with robust data-driven predictive control for connected and autonomous vehicles," in *2024 American Control Conference (ACC)*. IEEE, 2024, pp. 2266–2272.
- [52] B. Schürmann, M. Klischat, N. Kochdumper, and M. Althoff, "Formal safety net control using backward reachability analysis," *IEEE Transactions on Automatic Control*, vol. 67, no. 11, pp. 5698–5713, 2021.
- [53] S. Li, C. Chen, H. Zheng, J. Wang, Q. Xu, and K. Li, "Robust data-enabled predictive leading cruise control via reachability analysis," in *2024 IEEE 22nd International Conference on Industrial Informatics (INDIN)*. IEEE, 2024, pp. 1–8.
- [54] A. Alanwar, A. Koch, F. Allgöwer, and K. H. Johansson, "Data-driven reachability analysis from noisy data," *IEEE Transactions on Automatic Control*, vol. 68, no. 5, pp. 3054–3069, 2023.
- [55] S. Li, H. Zheng, J. Wang, C. Chen, Q. Xu, J. Wang, and K. Li, "Influence of information flow topology and maximum platoon size on mixed traffic stability," *Transportation Research Part C: Emerging Technologies*, vol. 171, p. 104950, 2025.
- [56] X. Jin, W. M. Haddad, Z.-P. Jiang, and K. G. Vamvoudakis, "Adaptive control for mitigating sensor and actuator attacks in connected autonomous vehicle platoons," in *2018 IEEE Conference on Decision and Control (CDC)*. IEEE, 2018, pp. 2810–2815.
- [57] C. Fan, U. Mathur, S. Mitra, and M. Viswanathan, "Controller synthesis made real: Reach-avoid specifications and linear dynamics," in *International Conference on Computer Aided Verification*. Springer, 2018, pp. 347–366.
- [58] L. Khoshnevisan and X. Liu, "A secure adaptive resilient neural network-based control of heterogeneous connected automated vehicles subject to cyber attacks," *IEEE Transactions on Vehicular Technology*, pp. 1–11, 2025.
- [59] H.-T. Sun, C. Peng, X. Ge, and Z. Chen, "Secure event-triggered sliding control for path following of autonomous vehicles under sensor and actuator attacks," *IEEE Transactions on Intelligent Vehicles*, vol. 9, no. 1, pp. 981–992, 2023.
- [60] P. Song, Q. Yang, Z. Zhang, and D. Li, "Model-free event-triggered resilient control for discrete-time nonlinear systems under sparse actuator attacks via grhdp," *Nonlinear Dynamics*, vol. 113, no. 5, pp. 4077–4096, 2025.
- [61] M. Althoff, "Reachability analysis and its application to the safety assessment of autonomous cars," Ph.D. dissertation, Technische Universität München, 2010.
- [62] W. Kühn, "Rigorously computed orbits of dynamical systems without the wrapping effect," *Computing*, vol. 61, pp. 47–67, 1998.
- [63] H. J. Van Waarde, M. K. Camlibel, J. Eising, and H. L. Trentelman, "Quadratic matrix inequalities with applications to data-based control," *SIAM Journal on Control and Optimization*, vol. 61, no. 4, pp. 2251–2281, 2023.
- [64] D. Q. Mayne, M. M. Seron, and S. V. Raković, "Robust model predictive control of constrained linear systems with bounded disturbances," *Automatica*, vol. 41, no. 2, pp. 219–224, 2005.
- [65] M. Althoff, "Guaranteed state estimation in cora 2021," in *Proc. of the 8th International Workshop on Applied Verification of Continuous and Hybrid Systems*, 2021.
- [66] T. G. Reid, S. E. Houts, R. Cammarata, G. Mills, S. Agarwal, A. Vora, and G. Pandey, "Localization requirements for autonomous vehicles," *SAE International Journal of Connected and Automated Vehicles*, vol. 2, no. 12-02-03-0012, pp. 173–190, 2019.
- [67] D. P. Bowyer, R. Akçelik, and D. Biggs, *Guide to fuel consumption analyses for urban traffic management*, 1985, no. 32.
- [68] L. Huang, J. Coulson, J. Lygeros, and F. Dörfler, "Decentralized data-enabled predictive control for power system oscillation damping," *IEEE Transactions on Control Systems Technology*, vol. 30, no. 3, pp. 1065–1077, 2021.